Impact of atmospheric forcing uncertainties on Arctic and Antarctic sea ice simulation in CMIP6 OMIP

Xia Lin[1,2], François Massonnet[1], Thierry Fichefet[1], Martin Vancoppenolle[3]

[1]Georges Lemaître Centre for Earth and Climate Research, Earth and Life Institute, Université catholique de Louvain, Louvain-la-Neuve, 1348, Belgium

[2]Southern Marine Science and Engineering Guangdong Laboratory (Zhuhai), Zhuhai, 519000, China

[3]Laboratoire d'Océanographie et du Climat, CNRS/IRD/MNHN, Sorbonne Université, 75252, Paris, France

Correspondence to: Xia Lin (xia.lin@uclouvain.be)

10 **Abstract.** Atmospheric reanalyses are valuable datasets to drive ocean-sea ice general circulation model and to propose multi-decadal reconstructions of the ocean-sea ice system in polar regions. However, these reanalyses exhibit biases in these regions. It was previously found that the representation of Arctic and Antarctic sea ice in models participating in the Ocean Model Intercomparison Project Phase 2 (OMIP2, using the Japanese 55-year atmospheric reanalysis) was significantly more realistic than in the

15 OMIP1 (forced by atmospheric state from the Coordinated Ocean-ice Reference Experiments version 2, CORE-II). To understand why, we study the sea ice concentration budget and its relations to surface heat and momentum fluxes, as well as the connections between the simulated ice drift and the ice concentration, the ice thickness and the wind stress in a subset of three models (CMCC-CM2-SR5, MRI-ESM2-0, and NorESM2-LM). These three models are representative of the ensemble and are the

20 only ones to provide the tendencies of ice concentration attributed to dynamic and thermodynamic processes required for the ice concentration budget analysis. It is found that negative summer biases in high-ice concentration regions and positive biases in the Canadian Arctic Archipelago (CAA) and central Weddell Sea (CWS) regions are reduced from OMIP1 to OMIP2 due to surface heat fluxes changes. Net shortwave radiation fluxes provide key improvements in the Arctic interior, CAA and

25 CWS regions. There is also an influence of improved surface wind stress in OMIP2 giving better winter Antarctic ice concentration and the Arctic drift speed simulations near the ice edge. The ice velocity direction simulation in the Beaufort Gyre and the Pacific and Atlantic sectors of the Southern Ocean in OMIP2 are also improved owing to surface wind stress changes. This study provides clues on how improved atmospheric reanalysis products influence sea ice simulations. Our findings suggest that

30 attention should be paid to the radiation fluxes and winds in atmospheric reanalyses in polar regions.

1 Introduction

Sea ice is an important component of the polar climate system. At high latitudes, the presence of sea ice affects the exchanges of heat, momentum and freshwater fluxes between the atmosphere and the ocean. Sea ice has experienced dramatic changes during recent decades, especially in the Arctic where the total

35   sea ice extent dramatically decreased over the satellite observing period (Comiso et al. 2008; Stroeve and Notz, 2018). In the Antarctic, the total sea ice extent increased slightly, but statistically significantly, to a record high in 2014 and decreased dramatically to the lowest value in 2017 over the satellite record (Parkinson, 2019; Fogt et al., 2022). A record low sea ice extent was set in 2022 (Raphael and Handcock, 2022). Sea ice variability can drive changes in the atmospheric energy budget

40   and circulation (Krikken and Hazeleger, 2015; Smith et al., 2017, 2022), as well as surface fluxes into the ocean and ocean circulation (Haumann et al., 2016; Sévellec et al., 2017; Meneghello et al., 2018).

A good simulation of sea ice is crucial to improve model predictions and climate change projections. Yet, limitations still exist in both fully coupled climate models and ocean-sea ice models. For the Arctic,

45   the observed decline of sea ice cover lies within the spread of modeled trends, but the multi-model mean trend is underestimated in the third, fifth and sixth phases of the Coupled Model Intercomparison Project (CMIP, Stroeve et al. 2007; Massonnet et al. 2012; Rosenblum and Eisenman 2017; Notz and SIMIP Community, 2020). The observed accelerated ice drift speed is not captured in CMIP3 models (Rampal et al., 2011), while the accelerated ice drift speed is produced in winter but not in summer in

50   CMIP5 models (Tandon et al., 2018). Large ice edge and thickness errors in Arctic subregions are identified from the spatial distribution of sea ice in CMIP6 models (Stroeve et al. 2014; Watts et al., 2021). For the Antarctic, the CMIP5 and CMIP6 models fail to capture the slightly increase of observed ice extent from 1979 to 2015 and they do not properly simulate the mean state and interannual variability of the ice cover (Mahlstein et al., 2013; Turner et al, 2013; Zunz et al. 2013; Shu et al., 2015,

55   2020; Roach et al., 2020). Large biases are also noticed in simulations conducted with ocean-sea ice models driven by atmospheric reanalysis data, in particular on the Antarctic sea ice extent variability and the ice thickness and motion in both hemispheres (e.g., Massonnet et al. 2011; Lecomte et al., 2016; Chevallier et al. 2017). By performing sensitivity experiments with these ocean-sea ice models, one can gain some insight into the origins of those biases. The focus of the present study is to quantify and

60   understand how the sea ice simulation can be improved by changing atmospheric forcing fields in ocean-sea ice models.

Atmospheric reanalyses are particularly valuable in polar regions where in-situ observations are scarce. However, these reanalyses have their limitations and biases (e.g., Lindsay et al., 2014; Bromwich et al.,

65   2016; Barthélemy et al., 2018; Lin et al., 2018). Previous studies have shown that differences in the atmospheric forcing fields can affect the ocean-sea ice model simulations of the Arctic monthly mean

sea ice thickness and total sea ice volume (e.g., Hunke and Holland, 2007; Lindsay et al., 2014; Sterlin et al., 2021), the Arctic and Antarctic sea ice concentration in the marginal ice zones (Chaudhuri et al., 2016) as well as the Antarctic sea ice extent, motion and thickness (Barthélemy et al., 2018). Wu et al.

70   (2020) also showed the positive impacts of high-frequency (hourly to daily) atmospheric fluctuations on the Antarctic sea ice simulation, which implies that driving an ocean-sea ice model with a reanalysis that is developed at enhanced temporal and spatial resolution can help capture the small scale atmospheric processes and eventually improve the representation of sea ice.

75   The CMIP6 Ocean Model Intercomparison Project (OMIP, Griffies et al., 2016) provides global ocean-sea ice model simulations with a experimental setup under two different atmospheric forcings: the Coordinated Ocean-ice Reference Experiments, version 2 interannual forcing (CORE-II; Large and Yeager, 2009) and the updated Japanese 55-year atmospheric reanalysis (JRA55-do; Tsujino et al., 2018). The JRA55-do atmospheric forcing is relatively new with major improvements, e.g., increased

80   temporal frequency (3h) and horizontal resolution (0.5625°), compared to CORE-II forcing (6h and 1.875°). The Arctic and Antarctic sea ice concentration and drift simulations in CMIP6 OMIP2 models forced by JRA55-do are improved compared to those in OMIP1 models forced by CORE-II (Tsujino et al., 2020; Lin et al., 2021). This provides an opportunity to check the processes contributing to these improvements under changed atmospheric forcing in the OMIP models and to compare the sea ice

85   simulation differences in the Arctic and Antarctic.

The spatial variability of sea ice concentration and its links with the atmospheric circulation vary with season (Hu et al., 2002; Rigor et al., 2002; Renwick et al., 2012; Raphael and Hobbs, 2014). During the seasonal sea ice advance and retreat periods, the spatial ice concentration variability is associated with

90   different atmospheric circulation patterns and both thermal advection and dynamical forcing are important (Raphael and Hobbs, 2014). The thermodynamic and dynamic processes that contribute to the Antarctic sea ice concentration seasonal evolution are discussed in Barthélemy et al. (2018). These authors conducted three sensitivity experiments with different atmospheric forcing fields using the NEMO-LIM3 ocean-sea ice model. They found that differences in the thermodynamic component of

95   the forcing were mostly responsible for the differences in ice concentration simulated by the model experiments during the melting season, while during the ice expansion period, both thermodynamic and dynamic components were important. The relationships between spatially-averaged observed sea ice drift speed in the central Arctic and ice concentration, ice thickness and wind stress were investigated by Olason and Notz (2014). According to their results, on the seasonal time scales, ice drift speed

100   changes in the central Arctic are primarily attributable to the changes in the ice concentration from June to November and changes in the ice thickness when the ice concentration is high, i.e., from December to March. The relationships between Arctic sea ice drift speed, concentration and thickness are

The Cryosphere

Discussions

Open Access

EGU

relatively well captured by the NEMO-LIM3 model (Docquier et al., 2017) and the coupled model GFDL-ESM2G (Eyring et al., 2020), with higher drift speed associated with lower concentration and

105   thickness. In the Antarctic, away from the coastline, the mean ice drift is significantly correlated with the wind forcing in the Pacific and Atlantic sectors, with the spatially averaged vector correlation coefficient larger than 0.7 (Kimura, 2004; Holland and Kwok, 2012).

This paper complements a companion publication (Lin et al., 2021) that documents a new Sea Ice

110   Evaluation Tool (SITool v1.0) and applies this tool to assess the sea ice simulations in CMIP6 OMIP models. In that study, the improved Arctic and Antarctic ice concentration and drift simulations in CMIP6 OMIP2 compared to OMIP1 were highlighted from performance metrics and diagnostic spatial maps. In the present study, the thermodynamic and dynamic processes that contribute to the improved ice concentration simulation in OMIP2 compared to OMIP1 are assessed. The related surface sensible

115   and latent heat fluxes, net shortwave and longwave radiation fluxes, as well as surface wind stress on sea ice are investigated to trace the origin of simulated sea ice differences back to the forcing datasets. Meanwhile, the sensitivity of ice drift simulation to the changes in ice concentration, ice thickness and surface wind stress are examined to help understand the factors responsible for improving the ice drift simulation. This paper is organized as follows. The CMIP6 OMIP models and observational references

120   are described in Sect. 2. The sea ice concentration simulations and the effects of the thermodynamic and dynamic components of the atmospheric forcing are presented in Sect. 3.1. The ice drift simulation and the connections to ice concentration, ice thickness and wind stress are discussed in Sect. 3.2. Finally, in Sect. 4, conclusions and discussion are provided. Appendix A presents some extra sea ice diagnostics.

2 Models and observational references

125   Five CMIP6 OMIP models were forced by both CORE-II (OMIP1) and JRA55-do (OMIP2) reanalysis data so far, and they are marked as <model name + /C and /J>, such as CMCC-CM2-SR5/C and CMCC-CM2-SR5/J, respectively. Three of the five models (CMCC-CM2-SR5, MRI-ESM2-0, and NorESM2-LM) provide the tendencies of sea ice concentration attributed to dynamic vs. thermodynamic processes. The outputs from these three model groups are chosen to study the effects of

130   atmospheric forcing changes on the representation of the sea ice state. The surface heat fluxes (net sensible and latent heat fluxes and net shortwave and longwave radiation fluxes) and surface wind stress on sea ice from model outputs are used for diagnosis. The cross-metric analysis in Sect. 3.4 of Lin et al. (2021) shows that NorESM2-LM/J is the best performing model regarding ice concentration in both hemispheres, but the worst for ice drift. For the sake of readability and to not overload the manuscript,

135   figures of the main text focus on this model. The other two models do not show fundamentally different behavior when the atmospheric forcing is changed and the figures from these two models are available in Appendix A.

The observed sea ice concentration product NSIDC-0051 derived from the passive microwave data (Cavalieri et al., 1996), the ice thickness data derived from the measurements of ESA's Environmental Satellite (Envisat) radar altimeter (Guerreiro et al., 2017) and the ice drift product KIMURA derived from the AMSR-E data and processed by Kimura et al., (2013) are used for comparison. The evaluation period is chosen according to available historical model outputs and observations and is consistent with the analysis in Lin et al. (2021). The ice concentration, concentration tendencies and their relations to surface heat fluxes and wind stress are evaluated from 1980 to 2007, while the ice drift and its links to the ice concentration, ice thickness and wind stress are assessed from 2003 to 2007. More details on the CMIP6 OMIP models and observational references can be found in Sect. 2.2 of our previous paper (Lin et al., 2021).
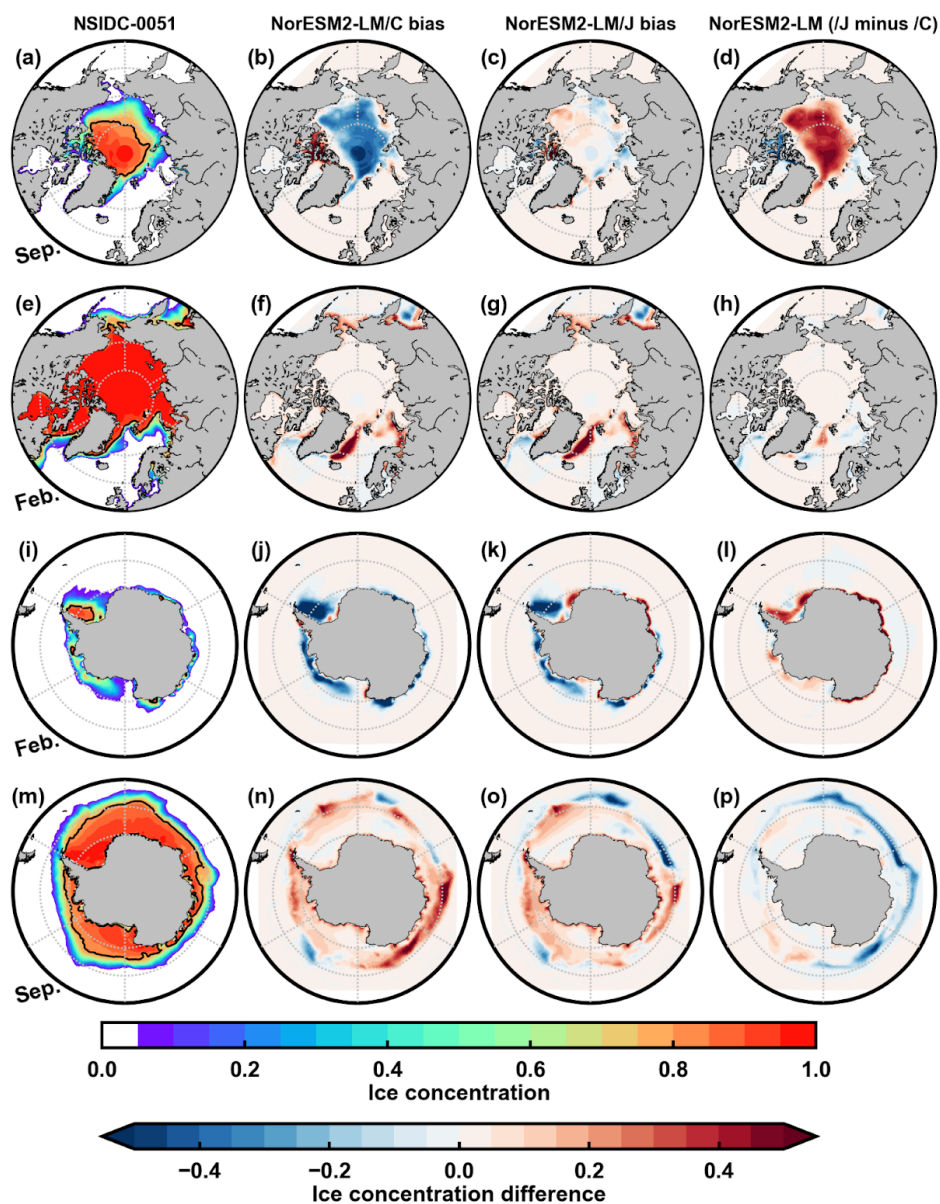
3 Results

3.1 Sea ice concentration

The 1980-2007 September and February mean spatial distribution of the Arctic and Antarctic sea ice concentration from the NorESM2-LM simulations compared to the satellite observational reference NSIDC-0051 are shown in Fig. 1 and figures from the CMCC-SR5-CM2 and MRI-ESM2-0 are displayed in Fig. A1. Olason and Notz (2014) suggested that, for concentrations above 80%, variations in sea ice state variables (concentration and thickness) can greatly affect the ice drift speed. To study the drivers of the ice concentration and drift speed changes, we divided the regions into two parts for each month, with ice concentration larger (interior) and smaller (exterior) than 80% in the NSIDC-0051 observational reference. The black lines in Fig. 1 exhibit September and February contours of 80% concentration in the NSIDC-0051 data. Spatial averages of the 1980-2007 September and February mean Arctic and Antarctic sea ice concentration biases are given in Table 1. The spatial averages over the interior and exterior regions are calculated with data closer than 75 km to the coast removed to reduce the spatial noise.

By applying the mean ice concentration difference metric developed in Lin et al. (2021), one finds that the Arctic mean ice concentration biases in OMIP1 simulations from 1980 to 2007 are reduced in OMIP2. The improvements are primarily in the boreal summer over the interior region and the Canadian Arctic Archipelago (CAA) region as shown in Fig. 1 and A1. In September, the spatial mean ice concentration biases in the interior region are reduced from -0.31 to 0.02 in NorESM2-LM and from -0.52 to -0.16 in CMCC-SR5-CM2 by changing the atmospheric forcing from CORE-II to JRA55-do (Table. 1). The reduced negative ice concentration bias in MRI-ESM2-0 is over the eastern part of the central Arctic Ocean. The spatial mean ice concentration bias in the interior region in MRI-ESM2-0/C (-0.03) is not weakened in MRI-ESM2-0/J (0.06). The positive ice concentration biases over the CAA

in three OMIP1 simulations are weakened in OMIP2 runs. The spatial mean ice concentration biases in the CAA are reduced from 0.26 to 0.07 in NorESM2-LM, from 0.1 to -0.03 in CMCC-SR5-CM2 and from 0.13 to 0.01 in MRI-ESM2-0 under changed forcing from CORE-II to JRA55-do. In February, the

175 ice concentration biases in exterior regions in three OMIP1 simulations are also present in OMIP2 runs, with minor reduction.

The Antarctic mean ice concentration biases in OMIP1 simulations from 1980 to 2007 are also diminished. The improvements are mainly over the coastal regions of the western Weddell Sea and the

180 Amundsen Sea in the austral summer and over exterior regions from 70° to 180°E in winter from OMIP1 to OMIP2 as shown in Fig. 1 and A1. In February, the spatial mean ice concentration biases in the interior region from 52° to 60°W are reduced from -0.71 to -0.41 in NorESM2-LM, from -0.68 to -0.51 in CMCC-SR5-CM2 and from -0.84 to -0.76 in MRI-ESM2-0 by changing the atmospheric forcing from CORE-II to JRA55-do (Table. 1). Positive ice concentration biases are shown in the central

185 Weddell Sea (CWS) in CMCC-SR5-CM2/C and MRI-ESM2-0/C but not in NorESM2-LM/C. The spatial mean ice concentration biases over the CWS are reduced from 0.36 to 0.22 in CMCC-SR5-CM2 and from 0.08 to 0.01 in MRI-ESM2-0 under changed forcing from CORE-II to JRA55-do. The NorESM2-LM exhibits a larger positive bias on the East Antarctic coast when forced by JRA55-do as compared with CORE-II. In September, the spatial mean ice concentration biases in exterior regions

190 from 70° to 180°E are reduced from 0.24 to 0.09 in NorESM2-LM, from 0.19 to 0.1 in CMCC-SR5-CM2 and from 0.33 to 0.2 in MRI-ESM2-0 under changed forcing from CORE-II to JRA55-do.

Figure 1. The 1980-2007 September and February mean Arctic (a to h) and Antarctic (i to p) sea ice concentration from the NSIDC-0051 data (first column), the differences between NorESM2-LM/C and NSIDC-0051 (second column), NorESM2-LM/J and NSIDC-0051 (third column), and NorESM2-LM/J and NorESM2-LM/C (fourth column). The black lines are contours of 80% concentration (a, e, i and m), which delineate the interior and exterior domains to compute spatial averages in Table 1.

Table 1. Spatial averages of the 1980-2007 September and February mean Arctic and Antarctic sea ice concentration (SIC) biases (vs. NSIDC-0051, Figs. 1, A1), as well as the ice concentration tendencies through thermodynamic and dynamic processes (Figs. 2, 3, A2 and A3), downward surface heat flux and stress on sea ice (Figs. 4, A4) over October-January and March-August. The results derived from three model groups under OMIP1 (/C) and OMIP2 (/J) runs are listed. The periods or regions on both sides of the slash (/) represent the Arctic and Antarctic, respectively. The spatial averages over the interior region in the Arctic and Antarctic (52° to 60°W), the Canadian Arctic Archipelago (CAA) and central Weddell Sea (CWS) in summer and over the exterior region in the Arctic (-45° to 90°E) and Antarctic (70° to 180°E) in winter are given. The improvements on ice concentration simulations and the related reasons in summer (bold) and winter (bold italic) are marked.

Variables	Periods & regions		Arctic			Antarctic		
			NorESM2-LM/C [/J]	CMCC-SR5-CM2/C [/J]	MRI-ESM2-0/C [/J]	NorESM2-LM/C [/J]	CMCC-SR5-CM2/C [/J]	MRI-ESM2-0/C [/J]
SIC bias	Summer (Sep./Feb.)	Interior	-0.31**[0.02]**	-0.52**[-0.16]**	-0.03[0.06]	-0.71**[-0.41]**	-0.68**[-0.51]**	-0.84**[-0.76]**
		CAA/CWS	0.26**[0.07]**	0.10**[-0.03]**	0.13**[0.01]**	0.005[0.003]	0.36**[0.22]**	0.08**[0.01]**
	Winter (Feb./Sep.)	Exterior	0.22[0.23]	0.16[0.13]	0.26[0.27]	0.24***[0.09]***	0.19***[0.1]***	0.33***[0.2]***
siconc tendency thermo. (10^{-3} day^{-1})	Mar.-Aug./Oct.-Jan.	Interior	-2.2**[0.6]**	-3.2**[-0.9]**	0.4[1.5]	-4.5**[-1.9]**	-5.2**[-2.9]**	-6.1**[-3.9]**
		CAA/CWS	-0.05**[-1.05]**	-0.7**[-1.4]**	1.0**[0.22]**	-6.1[-6.12]	-4.4**[-7.2]**	-3.0**[-5.2]**
	Oct.-Jan./Mar.-Aug.	Exterior	0.5[1.6]	-4.9[-2.5]	-2.3[-0.1]	1.1[2.7]	0.5[1.4]	3.1[4.2]
siconc tendency dyn. (10^{-3} day^{-1})	Mar.-Aug./Oct.-Jan.	Interior	-1.6[-1.9]	-1.4[-1.6]	-2.0[-2.2]	-1.2[-2.1]	-0.3[-1.2]	-1.3[-3]
		CAA/CWS	-1.6[-1.7]	-1.6[-1.63]	-2.1[-2.19]	-1.3[-1.33]	-1.0[-0.2]	-3.7[-2.6]
	Oct.-Jan./Mar.-Aug.	Exterior	3.8[2.7]	8.6[6.1]	6.4[4.3]	2.9***[0.5]***	3.1***[1.7]***	1.2***[-0.6]***
downward surface heat flux on sea ice (W m^{-2})	Mar.-Aug./Oct.-Jan.	Interior	27.4**[14]**	32.9**[19.1]**	/	32.4**[23.1]**	31.6**[27.8]**	/
		CAA/CWS	24.5**[40.2]**	28.7**[46.2]**	/	7.1**[26.3]**	4.6**[34.1]**	/
	Oct.-Jan./Mar.-Aug.	Exterior	-21.8[-23.1]	-13.1[-16]	/	-19.5[-16.3]	-14.1[-6.5]	/
surface stress on sea ice (10^{-3} N m^{-2})	Mar.-Aug./Oct.-Jan.	Interior	11.9[12.6]	11.5[12.3]	12.2[12.6]	24.3[24.9]	24.6[25]	31.3[26.5]
		CAA/CWS	16.6[16.8]	17.4[18.9]	19.8[20.3]	26.8[25.3]	35.1[29.1]	41.9[39.6]
	Oct.-Jan./Mar.-Aug.	Exterior	57.1[55.3]	63.6[51.4]	148.5[123.1]	29.1***[22.7]***	20.4***[18.5]***	75.5***[68.8]***

3.1.1 The effects of thermodynamic vs. dynamic processes to ice concentration tendencies

To understand the differences in the simulated sea ice concentration noted in Figs. 1 and A1, we analyze the thermodynamic and dynamic processes contributing to the concentration tendencies during

The Cryosphere
Discussions
Open Access
EGU

215 the melt and growth seasons under different atmospheric forcings (Figs. 2, 3, A2, A3). The idea is close
to the sea ice concentration budget proposed in Holland and Kwok (2012) and applied in Uotila et al.
(2014), Lecomte et al. (2016) and Barthélemy et al. (2018). The contributing thermodynamic processes
to the concentration tendencies are freezing or melting, whereas the relevant dynamic processes are ice
advection, divergence/convergence and mechanical redistribution (rafting/ridging). The tendencies of
220 ice concentration due to dynamic and thermodynamic processes are available as standard SIMIP
diagnostics in the three models (Notz et al., 2016). Spatial averages of the ice concentration tendencies
are listed in Table 1, split per hemisphere, period and type of process (thermodynamics vs dynamics).

Compared to OMIP1 runs, changes in thermodynamic processes in the Arctic Ocean and the CAA
225 region contribute to the ice concentration changes in OMIP2 runs during March to August (Figs. 2 and
A2). The differences between OMIP1 and OMIP2 simulations on the contribution from dynamic
processes are small. As shown in Table 1, the spatial mean ice concentration tendencies due to
thermodynamic processes (unit: 10^{-3} day^{-1}) from OMIP1 to OMIP2 simulations are increased in the
interior region (from -2.2 to 0.6 in NorESM2-LM and -3.2 to -0.9 in CMCC-SR5-CM2) and decreased
230 in the CAA (from -0.05 to -1.05 in NorESM2-LM, -0.7 to -1.4 CMCC-SR5-CM2 and 1.0 to 0.22 in
MRI-ESM2-0). This is consistent with the reduced September Arctic ice concentration biases in OMIP2
runs (Figs. 1b to d, A1a to f). That is, by changing the atmospheric forcing from CORE-II to JRA55-do,
the simulations of Arctic summer ice concentration in the Arctic Ocean and the CAA region are
improved owing to a better representation of the thermodynamic processes. The thermodynamic
235 processes in MRI-ESM2-0/C contribute to the increase of ice concentration in the Beaufort Gyre region
(Fig. A2e) but not the decrease in the other two models (Figs. 2b and A2b) during March to August.
This explains why the large negative ice concentration biases in the Beaufort Gyre region in the other
two models are not present in MRI-ESM2-0/C (Figs 1b to d, A1a to f).

240 The major Arctic winter ice concentration biases are located in the exterior regions in OMIP1
simulations, with a minor reduction in OMIP2 runs (Figs. 1f to h, A1g to l). The winter ice
concentration simulation in exterior regions is complicated because both dynamic and thermodynamic
processes are important. The contributions from thermodynamic and dynamic processes are anti-
correlated in these regions, with the dynamic processes increasing ice concentration through the
245 expansion of sea ice and the thermodynamic processes contributing to ice melt. During October to
January, the increased Arctic ice concentration is dominated by dynamic processes in exterior regions in
OMIP1 simulations (Fig. 2 and A2). Compared to OMIP1 runs, these dynamic processes in OMIP2 runs
contribute to the decreased ice concentration in exterior regions on the east of Greenland, while
thermodynamic processes contribute to the increased ice concentration (see also Table 1). This
250 contributes to minor winter ice concentration differences between OMIP1 and OMIP2 simulations.

During October to January, the thermodynamic processes contribute to the decreased ice concentration in the Southern Ocean, except in some coastal regions, and the dynamic processes contribute to the decreased ice concentration in the inner region in the three OMIP1 runs (Figs. 3 and A3). Compared to OMIP1 runs, the thermodynamic processes dominate the increased ice concentration in the coastal

255   regions of the western Weddell Sea and Amundsen Sea in the three OMIP2 simulations, as well as the decreased ice concentration in the CWS in CMCC-SR5-CM2/J and MRI-ESM2-0/J. As shown in Table 1, the spatial mean ice concentration tendency due to thermodynamic processes (unit: 10^{-3} day^{-1}) from OMIP1 to OMIP2 simulations is increased in the interior region from 52° to 60°W (from -4.5 to -1.9 in NorESM2-LM, -5.2 to -2.9 in CMCC-SR5-CM2 and -6.1 to -3.9 in MRI-ESM2-0) and decreased in the

260   CWS (from -4.4 to -7.2 in CMCC-SR5-CM2 and -3.0 to -5.2 in MRI-ESM2-0). This is consistent with the reduced February Antarctic ice concentration biases in OMIP2 runs (Figs. 1j to l, A1m to r). The positive bias in the coastal region of the East Antarctic sector in the NorESM2-LM/J simulation (Figs. 1k) is related to thermodynamic processes (Fig. 3e). By changing the atmospheric forcing from CORE-II to JRA55-do, the simulations of Antarctic summer ice concentration in the coastal regions of the

265   western Weddell Sea and the Amundsen Sea, as well as the CWS region, are improved owing to the thermodynamic processes.

During March to August, the thermodynamic processes contribute to the increased Antarctic ice concentration, except for some exterior regions, and the dynamic processes contribute to the increased

270   ice concentration primarily in the exterior region (Figs. 3 and A3). Compared to OMIP1 runs, the dynamic processes dominate the decreased ice concentration in exterior regions in the three OMIP2 simulations. As shown in Table 1, the spatial mean ice concentration tendencies related to dynamic processes (unit: 10^{-3} day^{-1}) from OMIP1 to OMIP2 simulations are decreased in the exterior region from 70° to 180°E (from 2.9 to 0.5 in NorESM2-LM, 3.1 to 1.7 in CMCC-SR5-CM2 and 1.2 to -0.6 in MRI-

275   ESM2-0). This is consistent with the reduced September Antarctic ice concentration biases from 70° to 180°E in OMIP2 runs (Figs. 1n to p, A1s to x). The simulations of the Antarctic winter ice concentration in the exterior region from 70° to 180°E are improved due to the dynamic processes when forced by JRA55-do as compared with CORE-II.

280   In general, by changing the atmospheric forcing from CORE-II to JRA55-do, the improvements in the simulation of summer Arctic and Antarctic sea ice concentration within the pack are driven by differences in the thermodynamic tendency terms, while the improvements in Antarctic winter concentration simulation in the exterior region from 70° to 180°E are dominated by differences in dynamic tendency terms. For other cases (winter Arctic ice concentration in the exterior region, ice

285   concentration in coastal regions), improvements are not as clear.
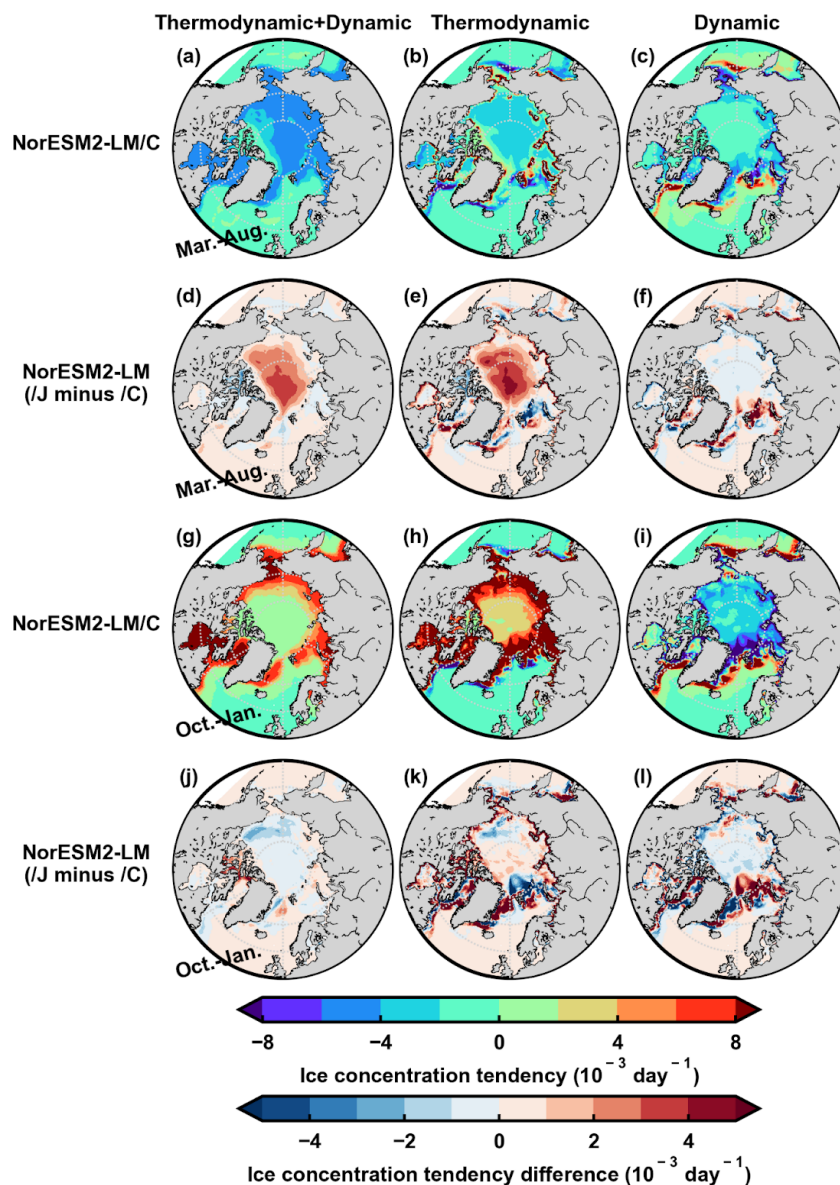
Figure 2. The 1980-2007 March-August (a to f) and October-January (g to l) mean Arctic sea ice concentration tendencies in NorESM2-LM/C (a to c, g to i) and the differences between NorESM2-LM/J and NorESM2-LM/C (d to f, j to l). The ice concentration tendencies due to thermodynamic and dynamic processes in total are in the first column, and individual contributions are in the second and third columns.
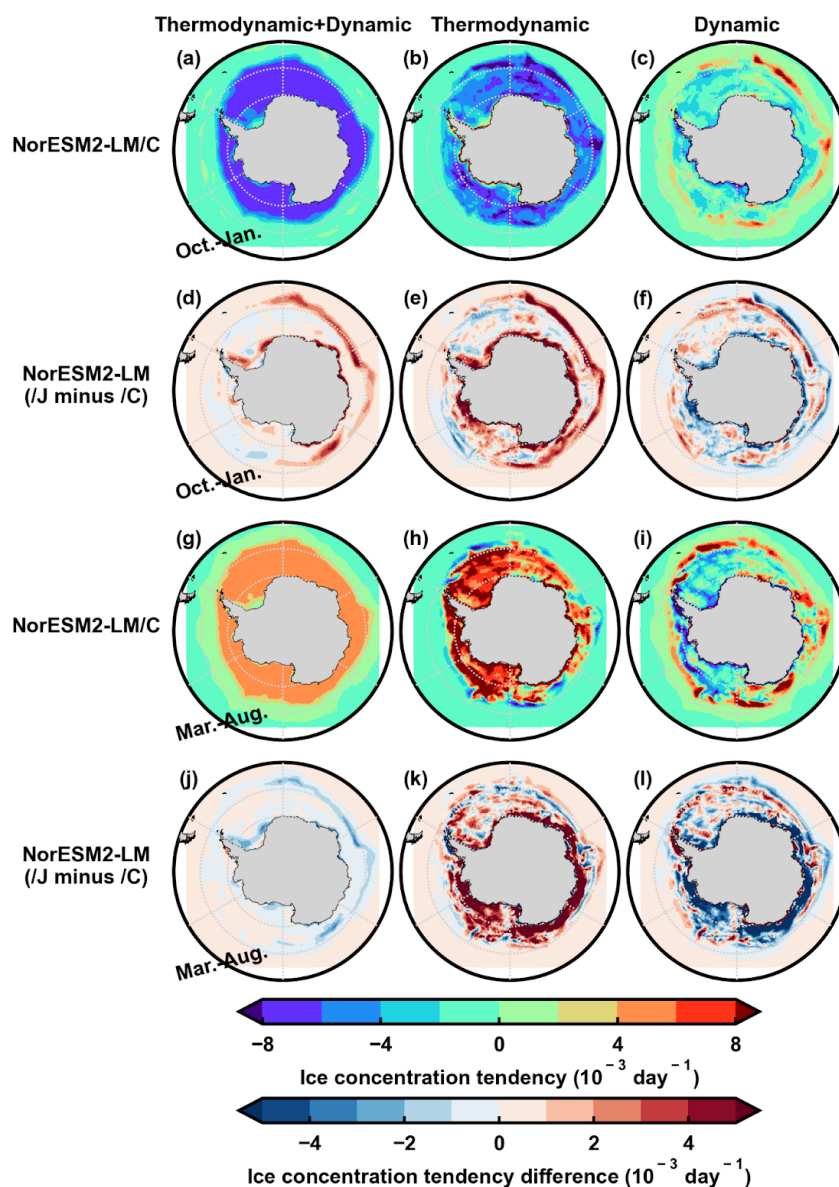
Figure 3. Same as Fig. 2 but for the 1980-2007 October-January (a to f) and March-August (g to l) mean Antarctic sea ice concentration tendencies.

295 **3.1.2 Surface heat and momentum flux**

To trace the origin of the differences in thermodynamic and dynamic tendency terms noted in the previous section, the surface heat and momentum fluxes available from the standard OMIP1 and OMIP2 model outputs are compared. The surface heat fluxes are not provided in MRI-ESM2-0. The sign convention for flux in this study is that a downward flux towards the surface is positive. The net

300 surface heat flux is downward (positive) in the Arctic during March to August and in the Antarctic

during October to January in OMIP1 runs (Figs. 4 and A4). Compared to OMIP1 simulations, the downward net surface heat fluxes in OMIP2 simulations are smaller in the central Arctic Ocean and over the coastal regions of the western Weddell Sea, and larger in the CAA and CWS regions. As shown in Table 1, the spatial mean downward net surface heat flux from OMIP1 to OMIP2 simulations

305   is decreased in the Arctic interior region (from 27.4 to 14 W m^{-2} in NorESM2-LM and 32.9 to 19.1 W m^{-2} in CMCC-SR5-CM2) and in the Antarctic interior region from 52° to 60°W (from 32.4 to 23.1 W m^{-2} in NorESM2-LM and 31.6 to 27.8 W m^{-2} in CMCC-SR5-CM2), and increased in the CAA region (from 24.5 to 40.2 W m^{-2} in NorESM2-LM and 28.7 to 46.2 W m^{-2} in CMCC-SR5-CM2) and the CWS region (from 7.1 to 26.3 W m^{-2} in NorESM2-LM and 4.6 to 34.1 W m^{-2} in CMCC-SR5-CM2). The

310   downward net surface heat flux changes in OMIP2 simulations contribute to the improved ice concentration simulation in those regions (Figs. 1 and A1).

To study which part dominates the downward net surface heat flux changes from OMIP1 to OMIP2 simulations, the surface sensible and latent heat fluxes and the net shortwave and longwave radiation

315   fluxes are computed (Figs. 5 and A5). Compared to OMIP1 simulations, the downward net shortwave radiation flux and latent heat flux in OMIP2 are smaller in the central Arctic Ocean and the coastal region of the western Weddell Sea, the downward net shortwave radiation flux is larger in the CAA and CWS regions and the sensible heat flux is larger in the CAA region. As shown in Table 2, the decreased downward net shortwave radiation flux in OMIP2 simulations (-13.4 W m^{-2} in NorESM2-LM and -12.7

320   W m^{-2} in CMCC-SR5-CM2) dominates the net surface heat flux changes in the central Arctic Ocean. The decreased latent heat flux in OMIP2 simulations (-12.6 W m^{-2} in NorESM2-LM and -13.1 W m^{-2} in CMCC-SR5-CM2) dominates the net surface heat flux changes in the coastal region of the western Weddell Sea. In the CAA region, the increased downward net shortwave radiation flux and sensible heat flux in OMIP2 simulations (16.1 and 10.0 W m^{-2} in NorESM2-LM, 14.9 and 13.6 W m^{-2} in

325   CMCC-SR5-CM2) dictate the net surface heat flux changes. In the CWS region, the increased downward net shortwave radiation flux (19.9 W m^{-2} in NorESM2-LM and 39.2 W m^{-2} in CMCC-SR5-CM2) is the major contributor to the net surface heat flux changes.

The changes in the shortwave radiation flux are crucial for the summer ice concentration changes in the

330   OMIP2 simulations in the Arctic interior region and the CAA and CWS regions. The downward and upward shortwave radiation fluxes in NorESM2-LM and CMCC-SR5-CM2 (Fig. A6) as well as spatial averages (Table 2) are displayed. The decreased downward shortwave radiation flux in OMIP2 simulations (-9.6 W m^{-2} in NorESM2-LM and -9.9 W m^{-2} in CMCC-SR5-CM2) is mostly responsible for the net shortwave radiation flux changes in the central Arctic Ocean. The increased net shortwave

335   radiation fluxes in the CAA and CWS regions are related to the increased downward and decreased upward shortwave radiation flux in OMIP2 simulations.
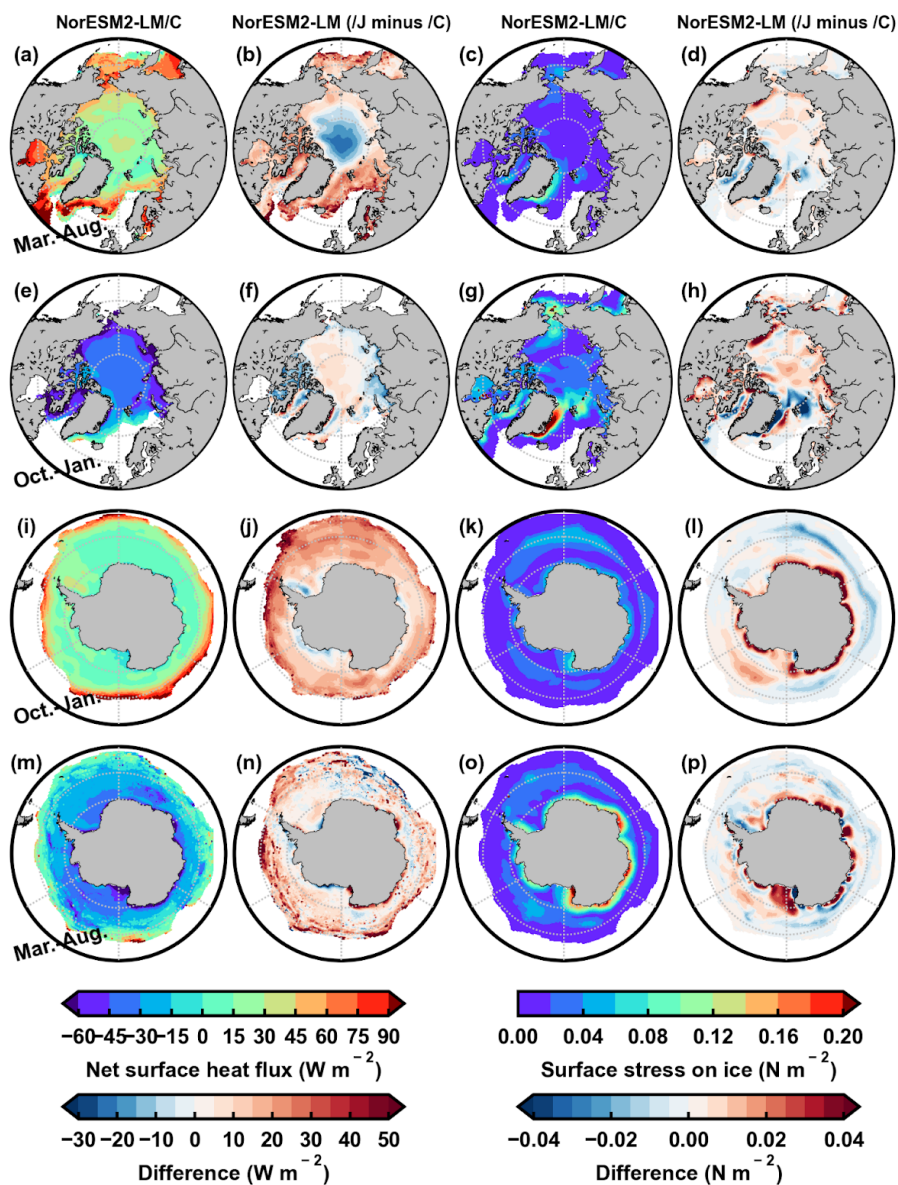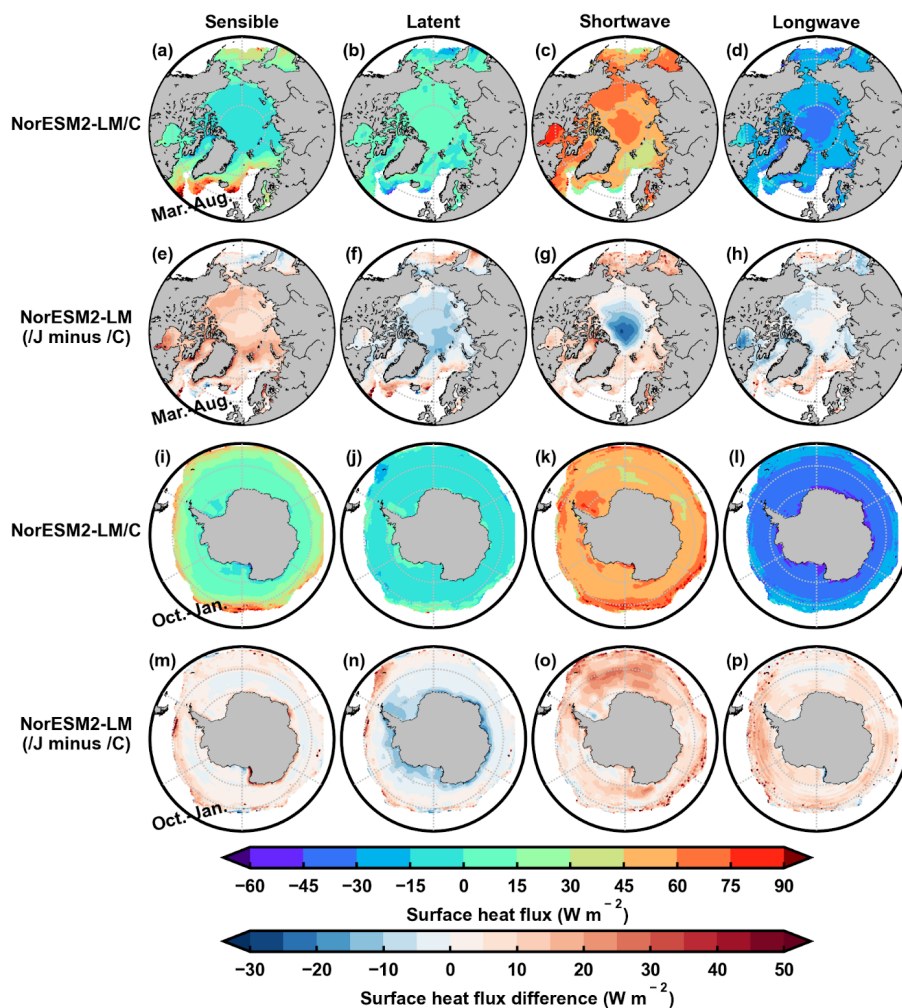
Figure 4. The 1980-2007 March-August and October-January mean Arctic (a to h) and Antarctic (i to p) net surface heat flux (first two columns) and surface stress (last two columns) on sea ice. The first and third columns correspond to NorESM2-LM/C, and the second and fourth columns are differences between NorESM2-LM/J and NorESM2-LM/C. The positive values indicate a net flux downward.

14

Figure 5. The 1980-2007 March-August mean Arctic (a to h) and October-January mean Antarctic (i to p) surface sensible (first column) and latent heat fluxes (second column), net shortwave (third column) and longwave radiation fluxes (fourth column). The first and third rows correspond to NorESM2-LM/C, and the second and fourth rows are differences between NorESM2-LM/J and NorESM2-LM/C. The positive values indicate a net flux downward.

Compared to other regions, the surface stress on ice along the east coasts of Greenland, Svalbard and Baffin Island, near the Bering Strait from 60 to 70°N, in the Antarctic coastal regions and inside the subpolar gyres is larger in OMIP1 simulations (third column in Fig. 4 and third and fifth columns in Fig. A4). This contributes to the smaller ice concentration due to the dynamic processes in those regions (Figs. 2, 3, A2 and A3). The large winter concentration biases in both hemispheres are located in exterior regions. In wintertime, the reduced Antarctic ice concentration biases in the exterior region from 70° to 180°E in OMIP2 simulations are dominated by the dynamic processes, as discussed in the previous section (Figs. 3 and A3). Compared to OMIP1 simulations, the surface wind stress on

15

Antarctic sea ice in OMIP2 simulations is weaker in the inner part of the exterior region from 70° to 180°E (Figs. 4o and p, A4u to x). As shown in Table 1, the spatial mean surface wind stress on sea ice

360   is decreased from OMIP1 to OMIP2 simulations in the exterior region from 70° to 180°E (from 29.1 to 22.7 N m^{-2} in NorESM2-LM and 20.4 to 18.5 N m^{-2} in CMCC-SR5-CM2 and 75.5 to 68.8 N m^{-2} in MRI-ESM2-0). The decreased surface wind stress in OMIP2 simulations in the inner part of the exterior region weakens the ice motion and reduces the ice concentration in the exterior region from 70° to 180°E.

365

Table 2. Same as Table 1 but for the spatial averages of the 1980-2007 mean Arctic (March-August) and Antarctic (October-January) net surface heat flux (Figs. 4 and A4), sensible and latent heat flux, net shortwave and longwave radiation flux (Figs. 5 and A5), as well as downward and upward shortwave flux (Figs. A6) over the interior region in the Arctic and Antarctic (52° to 60°W), the CAA and CWS

370   regions. The results derived from three model groups under OMIP1 (/C) and differences between OMIP2 and OMIP1 runs ([J-C]) are listed.

Periods & regions	Variables (W m^{-2}) downward positive	Arctic				Antarctic			
		NorESM2-LM /C [J-C]		CMCC-SR5-CM2 /C [J-C]		NorESM2-LM /C [J-C]		CMCC-SR5-CM2 /C [J-C]	
Interior	net surface heat flux	27.4**[-13.4]**		32.9**[-13.8]**		32.4**[-9.3]**		31.6**[-3.8]**	
	sensible	-7.0[10.9]		-6.9[10.3]		2.7[2.2]		5.4[1.1]	
	latent	4.8[-9.2]		4.6[-9.6]		0.8**[-12.6]**		1.7**[-13.1]**	
	net shortwave	60.8**[-13.4]**		66.4**[-12.7]**		71.5[-4.2]		66.5[3.3]	
	downward shortwave / upward shortwave	177.7 **[-9.6]**	-116.9 [-3.81]	178.8 **[-9.9]**	-112.5 [-2.8]	238.2 [0.5]	-166.6 [-4.7]	237.6 [0.6]	-171.1 [2.7]
	net longwave	-31.2[-1.7]		-31.2[-1.8]		-42.5[5.2]		-41.9[4.9]	
CAA/CWS	net surface heat flux	24.5**[15.7]**		28.7**[17.5]**		7.1**[19.2]**		4.6**[29.5]**	
	sensible	-6.6**[16.1]**		-5.6**[14.9]**		8.5[-0.14]		13.1[-4.0]	
	latent	5.2[-6.9]		5.2[-7.4]		-10.5[-2.39]		-8.2[-5.1]	
	net shortwave	53.6**[10.0]**		56.5**[13.6]**		46.2**[19.9]**		34.3**[39.2]**	
	downward shortwave / upward shortwave	172.7 [6.0]	-119.1 [4.0]	173.3 [4.5]	-116.8 [9.1]	215.0 [9.8]	-168.8 [10.2]	213.5 [10.2]	-179.2 [29.0]
	net longwave	-27.7[-3.4]		-27.4[-3.5]		-37.1[1.8]		-34.5[-0.65]	

The improvement in the winter Arctic ice concentration in the exterior region is not as clear. Compared to OMIP1 simulations, the surface wind stress in OMIP2 simulations is smaller along the east coasts of Greenland, Svalbard and Baffin Island (Figs. 4g and h, A4i to l). This is consistent with the decrease of

375   ice concentration in the exterior region in OMIP2 simulations due to the dynamic processes away from the east coast (Figs. 2l, A2u and A2x). However, the thermodynamic processes in OMIP2 simulations contribute to the increase in ice concentration, which is close to the decrease due to the dynamic processes in these regions (Figs. 2k, A2t and A2w). The different contributions of the thermodynamic processes to the winter ice concentration tendency in the exterior region between OMIP1 and OMIP2

380   simulations are primarily related to the dynamic processes, while the surface heat flux difference on the sea ice is small.

3.2 Sea ice drift

3.2.1 Ice drift speed and its links with ice concentration, ice thickness and wind stress

The Arctic and Antarctic ice drift speed and direction simulations are improved from OMIP1 to OMIP2

385   (Lin et al., 2021). To understand the factors responsible for this feature, the sensitivity of the ice drift simulation to the changes in ice concentration, ice thickness and surface wind stress is investigated. The ice drift evaluation is performed for the exterior and interior regions with ice-free drift or not, based on the ice concentration. Spatial averages are computed for the interior and exterior regions in each hemisphere and different months. The simulated monthly mean and spatially averaged values of the ice

390   mean kinetic energy (MKE) and their links with the ice concentration, ice thickness as well as surface wind stress are examined for NorESM2-LM (Arctic in Fig. 6 and Antarctic in Fig. 7) and CMCC-CM2-SR5 and MRI-ESM2-0 (Arctic in Fig. A7 and Antarctic in Fig. A8).

In the Arctic interior region, the ice MKE in NorESM2-LM/C (Fig. 6a, light orange) is larger than that

395   in KIMURA data (light blue) and this positive bias is slightly reduced in NorESM2-LM/J (light green) from January to April, July and September. The largest improvement in the interior ice MKE occurs in September (Fig. 6b, black solid). It is mostly caused by the increased ice concentration and thickness in NorESM2-LM/J (Figs. 6c to f), the changes in the surface wind stress being very small (Figs. 6g to h). The Envisat dataset only extends to 81.5°N and the spatial average is not identical to the model mean

400   (up to 90°N), which can contribute to the smaller ice thickness in Envisat data (Fig. 6e, blue). Even though the ice concentration increase is the largest in August in NorESM2-LM/J (Fig. 6d, black solid), the change in ice drift speed is small in that month (Fig. 6b, black solid) due to the decreased ice thickness (Fig. 6f, black solid) and increased surface wind stress (Fig. 6h, black solid). In July, the increases in ice thickness and wind stress are close to that in September, while the decrease in drift

405   speed is small because the increase in ice concentration is smaller in July than that in September. Compared to the OMIP1 simulation, the Arctic interior ice drift speed from January to December is not

improved in CMCC-CM2-SR5/J (Figs. A7a and b), and the improvement is very small in MRI-ESM2-0/J (Fig. A8a and b). The improvement of the September ice MKE in NorESM2-LM/J is not present in CMCC-CM2-SR5/J and MRI-ESM2-0/J. This is due to the much smaller increase in September ice

410 thickness (less than 0.2 m) in CMCC-CM2-SR5/J (Fig. A7f, black solid) and a smaller increase in September ice concentration (less than 0.2) and thickness (less than 0.7 m) in MRI-ESM2-0/J (Figs. A8f and g, black solid) compared to the ice concentration (0.5) and thickness (1.3 m) increase in NorESM2-LM/J.
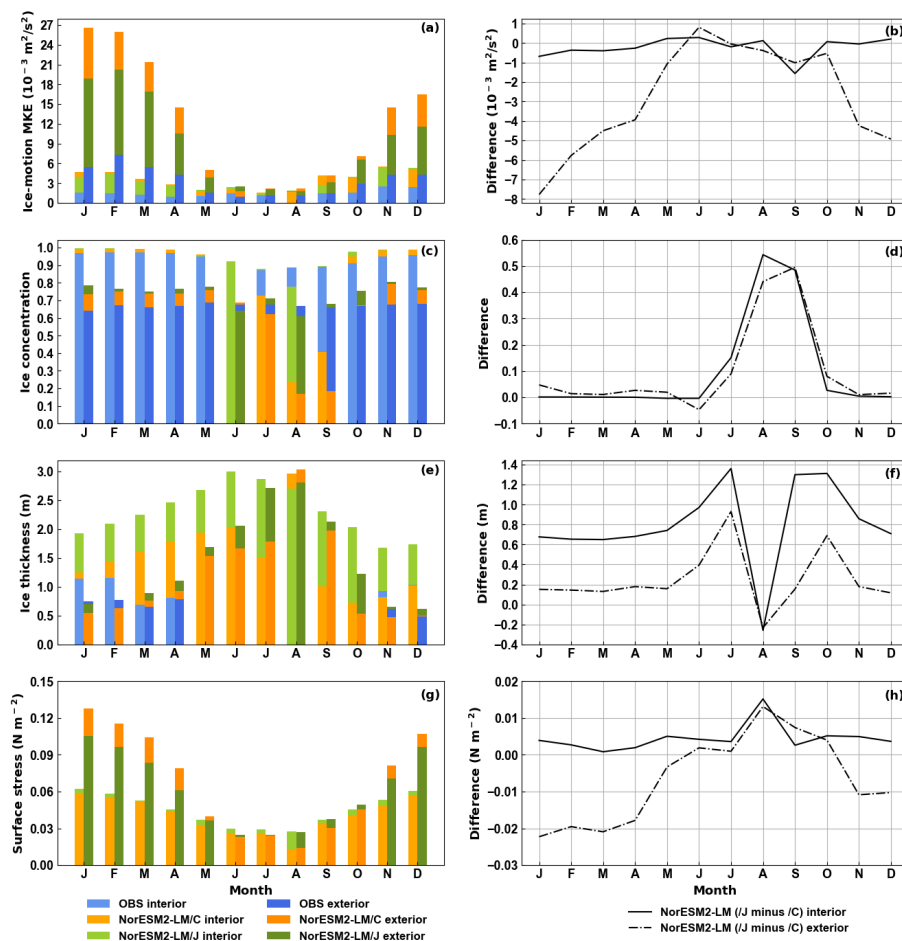
415 **Figure 6. Bar plots of 2003-2007 monthly mean and spatially averaged Arctic ice kinetic energy (MKE) (a), ice concentration (c), ice thickness (e) and surface wind stress (g) from observations (blue), NorESM2-LM/C (orange) and NorESM2-LM/J (green). These bars all start from zero. The observations of ice MKE, concentration and thickness are derived from KIMURA, NSIDC-0051 and Envisat data, respectively. The Envisat ice thickness data is provided from November to April and the coverage is limited up to 81.5°N. The left (light colors) and right (dark**

420 **colors) bars of each month are spatial averages on the regions with ice concentration larger (interior) and smaller (exterior) than 80% in NSIDC-0051, respectively. The differences between NorESM2-LM/J and NorESM2-LM/C ice MKE (b), ice concentration (d), ice thickness (f) and surface wind stress (h) in the interior (black solid) and exterior (dash-dotted) regions are shown.**

18

In the Arctic exterior region, the ice MKE in the three OMIP1 simulations (Figs. 6a, A7a and A8a, dark
425 orange) is much larger than that in KIMURA data (dark blue) and the positive biases in OMIP1
simulations are largely reduced in OMIP2 simulations (dark green) from November to April (Figs. 6b,
A7b and A8b, black dash-dotted). The decreased Arctic ice drift speed in OMIP2 simulations in the
exterior region from November to April is mainly induced by the decreased surface wind stress (Figs.
6g to h, A7g to h and A8g to h), the changes in ice concentration and thickness being very small (Figs.
430 6c to f, A7c to f and A8c to f).

In the Antarctic interior region, the ice MKE in NorESM2-LM/C (Fig. 7a, light orange) is larger than
that in KIMURA data (light blue) and this positive bias is reduced in March and April in NorESM2-
LM/J (light green). The decreased Antarctic ice drift speeds in the exterior region in March and April
435 (Fig. 7b, black solid) are consistent with the increased ice concentration and thickness in NorESM2-
LM/J (Fig. 7d and 7f, black solid). However, the ice concentration and thickness are also increased in
NorESM2-LM/J from December to February, similarly to April, while the ice MKE is not reduced. This
suggests that the ice motion at the beginning of the melting season is not that sensitive to the ice
concentration and thickness changes. Olason and Notz (2014) showed that the ice drift speed in April
440 and May is not correlated with ice concentration or thickness, and the increase in drift speed is due to
newly formed fractures without changes in ice concentration. It indicates that the not reduced Antarctic
ice MKE from December to February in NorESM2-LM/J can be related to newly formed fractures even
though the increases in ice concentration and thickness are similar to that in April. The ice MKE
positive bias is also reduced in March and April in CMCC-CM2-SR5/J and MRI-ESM2-0/J (Fig. A9b
445 and A10b, black solid) and changes in some other months are small. In CMCC-CM2-SR5/J and MRI-
ESM2-0/J, the reduced ice MKE is largely caused by increased ice concentrations in March and both
increased ice concentrations and thicknesses in April.

In the Antarctic exterior region, the ice MKE in NorESM2-LM/C is larger (Fig. 7a, dark orange) than
450 that in KIMURA data (dark blue) and this positive bias is reduced in NorESM2-LM/J (dark green) in
April and August (Fig. 7b, black dash-dotted, smaller than -1×10^{-3} m^2/s^2 as a baseline). The ice MKE
positive bias is reduced in April, June to September in CMCC-CM2-SR5/J, and August and September
in MRI-ESM2-0/J (Fig. A9a to b and A10a to b, black dash-dotted). In July and August, the ice MKE
positive bias in MRI-ESM2-0/C changes to a negative bias in MRI-ESM2-0/J, and the reduced bias in
455 July is not smaller than -1×10^{-3} m^2/s^2 (Figs. A10a). The reduced ice MKE in April in OMIP2
simulations is related to the increased ice concentration and thickness (Figs. 7d, f, A9d and A9f, black
dash-dotted), while the reduced ice MKE in August and September is dominated by the decreased wind
stress (Figs. 7h, A9h and A10h, black dash-dotted). The reduced positive bias of ice MKE in the

19

The Cryosphere
Discussions

Antarctic exterior region is much smaller than that in the Arctic in three OMIP2 simulations (Fig. 7b vs.

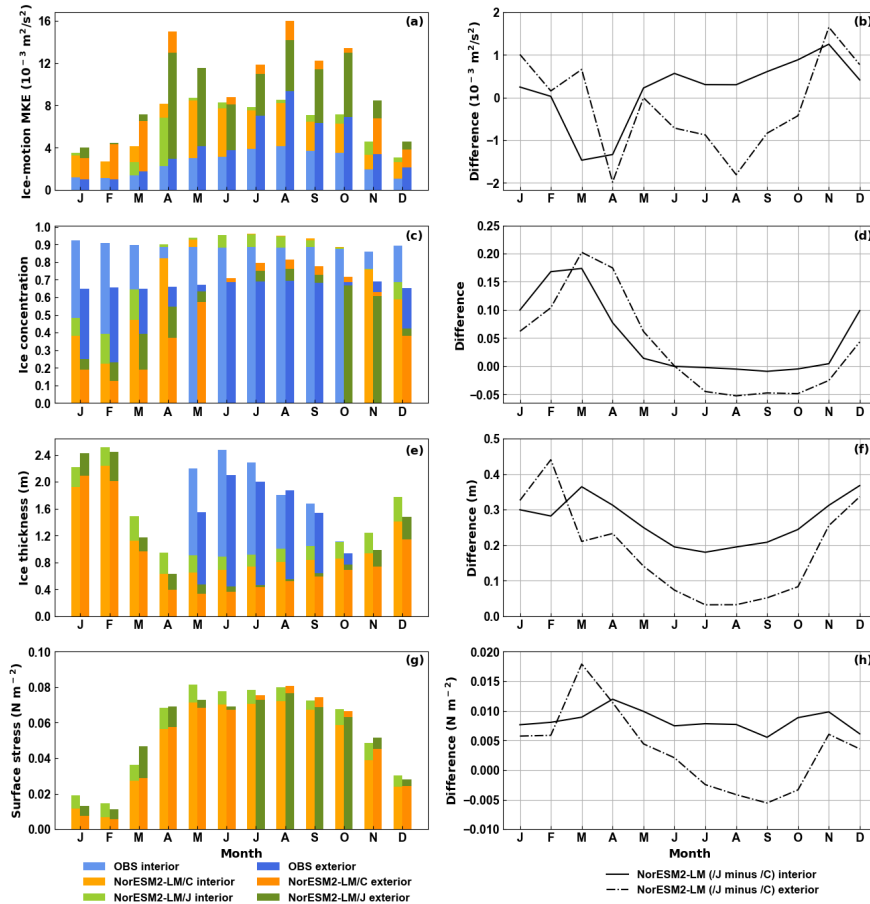460   6b, A9b vs. A7b and A10b vs. A8b, dash-dotted).

Figure 7. Same as Fig. 6 but for the Antarctic. The Envisat ice thickness data is provided from May to October.

3.2.2 Ice drift direction and its connections to wind stress

We finally aim at determining to what extent the change in atmospheric forcing may lead to an
465   improvement in the simulated ice drift direction (independently of the improvements in sea ice drift
speed noted in the previous section). To that end, the vector correlations between simulated and
observed ice drift fields (KIMURA data) are diagnosed, as done in Lin et al. (2021). In general, the
vector correlation coefficients between the modeled ice drift and KIMURA data during 2003–2007 are
larger in NorESM2-LM/J than that in NorESM2-LM/C in the Arctic (Figs. 8a to c) and Antarctic (Figs.
470   8g to i). The links with the surface wind stress are assessed. The vector correlation coefficients between
modeled ice drift and surface wind stress are much larger in NorESM2-LM/J than that in NorESM2-
LM/C in the Beaufort Gyre area (Fig. 8f) and the Pacific and Atlantic sectors of the Southern Ocean
(Fig. 8l). Those regions correspond to large improvements in the ice vector direction simulation in

NorESM2-LM/J (Fig. 8c and i). This suggests that the improved ice vector direction simulation is
475 related to the changed surface wind stress in NorESM2-LM/J. These improvements can also be found in
CMCC-CM2-SR5/J and MRI-ESM2-0/J (Fig. A11), but the improvements in MRI-ESM2-0/J are
smaller than that in NorESM2-LM/J and CMCC-CM2-SR5/J.
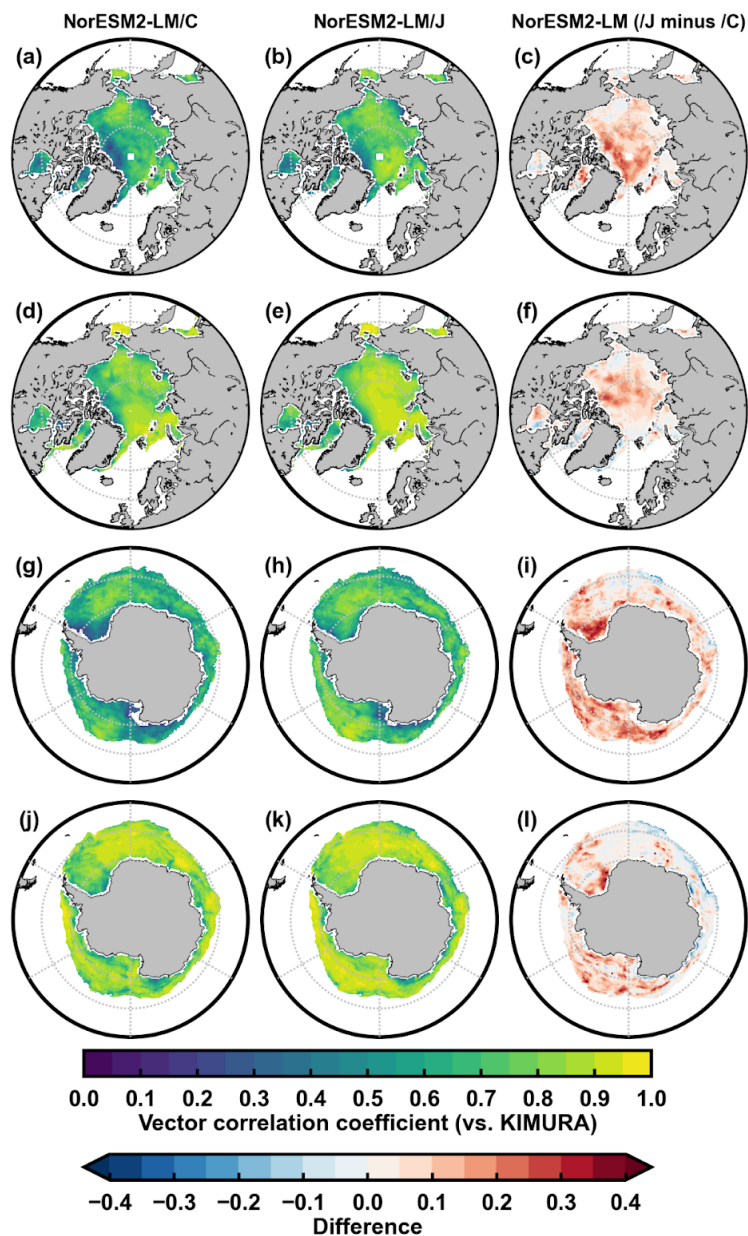
Figure 8. The significant vector correlation coefficients during 2003–2007 at a level of 99% between modeled ice drift
480 **(NorESM2-LM/C or /J) and KIMURA data in the Arctic (a and b) and Antarctic (g and h), and between modeled ice**
drift and surface wind stress in the Arctic (d and e) and Antarctic (j and k). The third column is the difference
between the second and first columns.

21

4 Conclusions and discussion

The OMIP provides useful datasets to reconstruct sea ice evolution over the past decades. Lin et al.
485 (2021) have shown that the accuracy of the reconstruction depends on the atmospheric forcing used.
This paper attempts to explain why this is so by conducting surface momentum and heat flux analyses.
The two atmospheric reanalysis products are different in both dynamical and thermodynamical
components for the Arctic and Antarctic, such as the air temperature and winds, which contribute to
heat flux and momentum flux differences in the ocean-sea ice models. We studied the dynamic and
490 thermodynamic processes contributing to the ice concentration tendencies and their links with surface
heat and momentum fluxes, as well as the connections between the simulated ice drift and the ice
concentration, ice thickness and wind stress.

In general, the sea ice concentration and drift speed and direction simulations are improved from
495 OMIP1 to OMIP2, and improvements in the Arctic are larger than that in the Antarctic. The net surface
heat fluxes are decreased in the interior region with ice concentration above 80% and increased in the
CAA and CWS regions during March to August (Arctic) and October to January (Antarctic) in OMIP2
compared to OMIP1 simulations. This can explain the improved OMIP2 ice concentration simulations
in the summer, pointing to the important role played by the thermodynamic processes during the ice
500 melting season. The changed net shortwave radiation fluxes from OMIP1 to OMIP2 simulations are
crucial to improve the OMIP2 summer ice concentration simulations in the Arctic interior, the CAA and
CWS regions. The decreased surface wind stress in the inner part of the exterior region during March to
August in OMIP2 compared to OMIP1 contributes to the improved (decreased) Antarctic September
OMIP2 ice concentration simulation in the exterior region from 70 to 180°E, pointing at the dominant
505 role of dynamic processes. The monthly mean and spatial averaged Arctic ice drift speed simulation in
the exterior region is improved (decreased) from November to April due to the decreased surface wind
stress in OMIP2 compared to OMIP1 simulations, while the improvement in the Antarctic is small. The
improved surface wind stress simulation in the Beaufort Gyre area and the Pacific and Atlantic sectors
of the Southern Ocean can help improve the ice vector direction simulation.
510

This study provides clues to improve the atmospheric reanalysis products for a better sea ice simulation
in ocean-sea ice models. The net shortwave radiation fluxes during the ice melting season in the interior
region and the wind stress during the ice expansion season in the exterior region are crucial for a better
sea ice concentration simulation. The wind stress is important to the sea ice drift speed and vector
515 direction simulations. More attention needs to be paid to the radiation fluxes and wind stress in the
atmospheric reanalysis products. Some aspects of the sea ice simulation are not that sensitive to the
atmospheric forcing changes, such as the winter Arctic ice concentration in the exterior region, ice
concentration in the coastal regions and ice drift speed in the exterior region. The limited impact of

atmospheric forcing on ice concentration simulation was also discussed in Barthélemy et al. (2018). In

520　these exterior and coastal regions, thermodynamic processes tend to compensate for the changes caused by dynamic processes and properly combined contributions from thermodynamic and dynamic processes are needed to improve the simulations. Both atmospheric forcing and model physics of the sea ice growth and melt processes are crucial for an improved simulation in these aspects. The collaborations with model development groups are needed to help advance the sea ice simulation.

525

While this paper reiterates the importance of the atmospheric forcing for the representation of the sea ice state, it is expected, based on the conclusions, that errors in the atmospheric forcing also affect the ocean through modified heat, freshwater and momentum fluxes between the ice and the ocean. These errors can thus eventually affect the representation of ocean temperature, salinity and currents.

530　**Appendix A**

In this appendix, extra sea ice diagnostics from CMCC-CM2-SR5 and MRI-ESM2-0 are given to help support the conclusions derived from NorESM2-LM. The ice concentrations from the simulations and their relationships to thermodynamical and dynamical processes in CMCC-CM2-SR5 and MRI-ESM2-0 are provided in Figs. A1 to A5. The surface heat flux on sea ice is not provided for MRI-ESM2-0 and

535　the corresponding figures are not included in Figs. A4 and A5. The downward and upward shortwave radiation flux in NorESM2-LM and CMCC-CM2-SR5 are added in Fig. A6. The ice drift simulation and the relationship to ice concentration, ice thickness and wind stress in CMCC-CM2-SR5 and MRI-ESM2-0 are provided in Figs. A7 to A11.
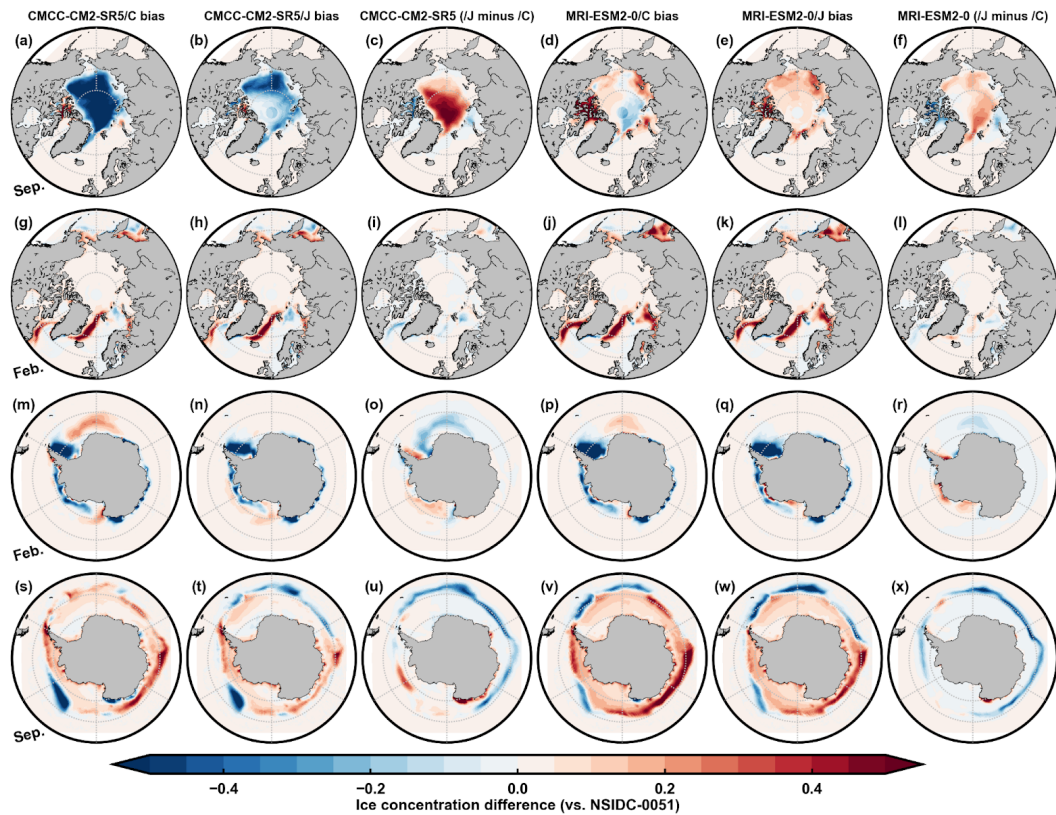
Figure A1. The 1980-2007 September and February mean Arctic (a to l) and Antarctic (m to x) sea ice concentration differences between CMCC-CM2-SR5/C and NSIDC-0051 (first column), CMCC-CM2-SR5/J and NSIDC-0051 (second column), CMCC-CM2-SR5/J and CMCC-CM2-SR5/C (third column), MRI-ESM2-0/C and NSIDC-0051 (fourth column), MRI-ESM2-0/J and NSIDC-0051 (fifth column), and MRI-ESM2-0/J and MRI-ESM2-0/C (sixth column).
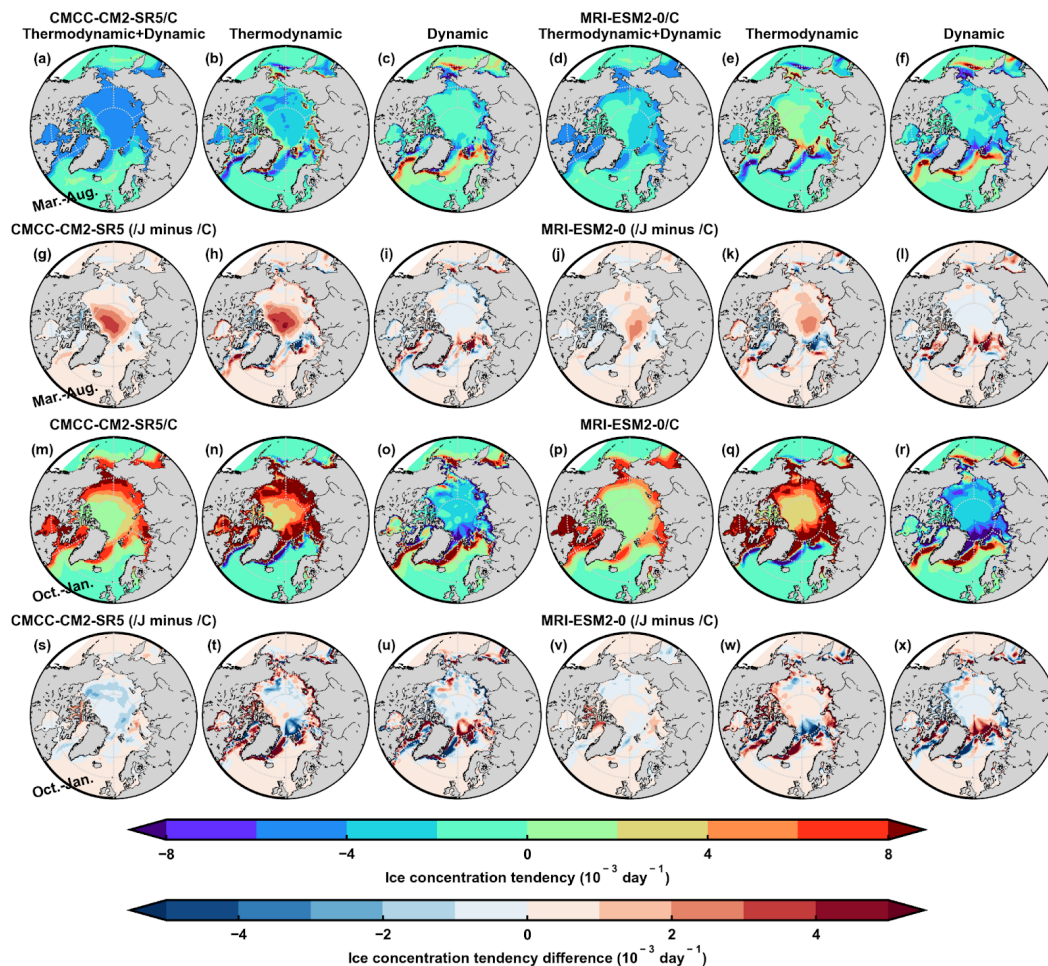
Figure A2. The 1980-2007 March-August (a to l) and October-January (m to x) mean Arctic sea ice concentration tendencies in CMCC-CM2-SR5 (first three columns) and MRI-ESM2-0 (last three columns) due to thermodynamic and dynamic processes in total (first and fourth columns), thermodynamic processes (second and fifth columns) and dynamic processes (third and sixth columns). The first and third rows are from CMCC-CM2-SR5/C and MRI-ESM2-0/C, and the second and fourth rows are differences between CMCC-CM2-SR5/J and CMCC-CM2-SR5/C, and between MRI-ESM2-0/J and MRI-ESM2-0/C, respectively.
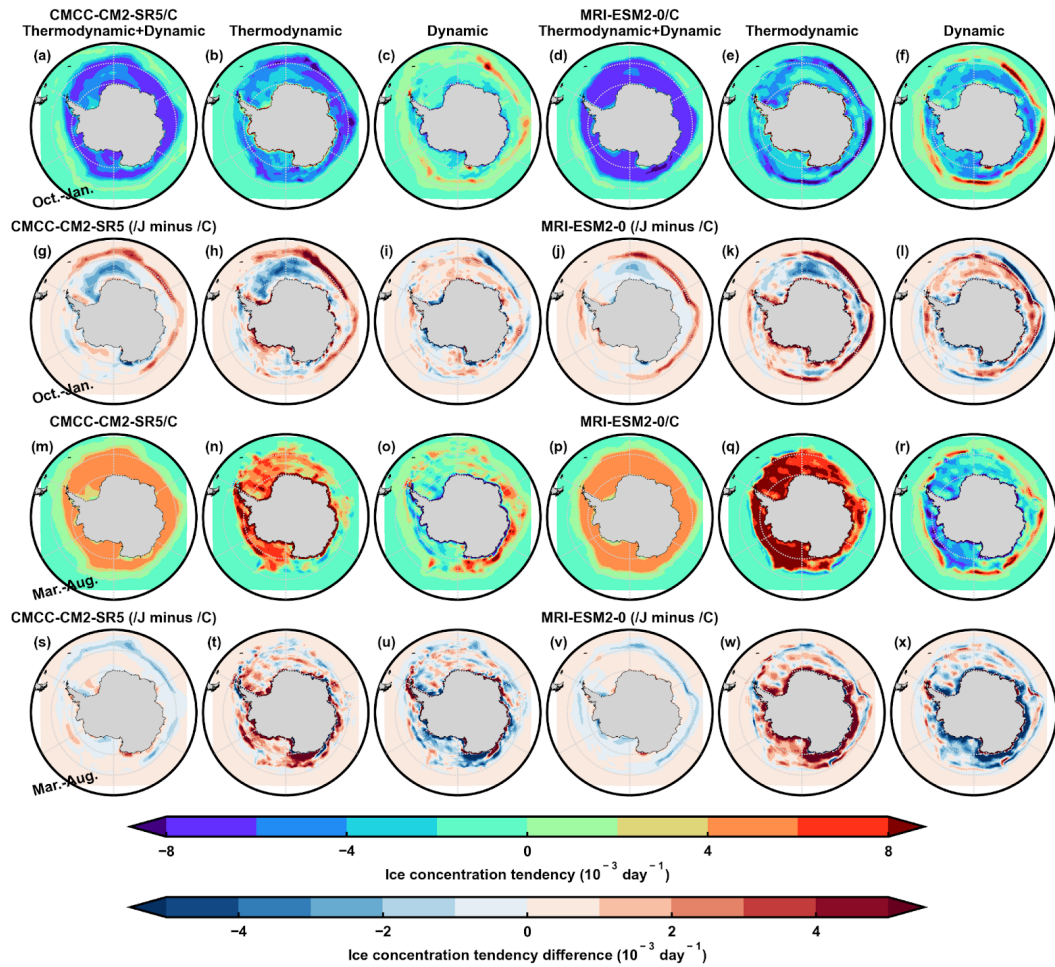
Figure A3. Same as Fig. A2 but for the 1980-2007 October-January (a to l) and March-August (m to x) mean

555 **Antarctic sea ice concentration tendencies.**
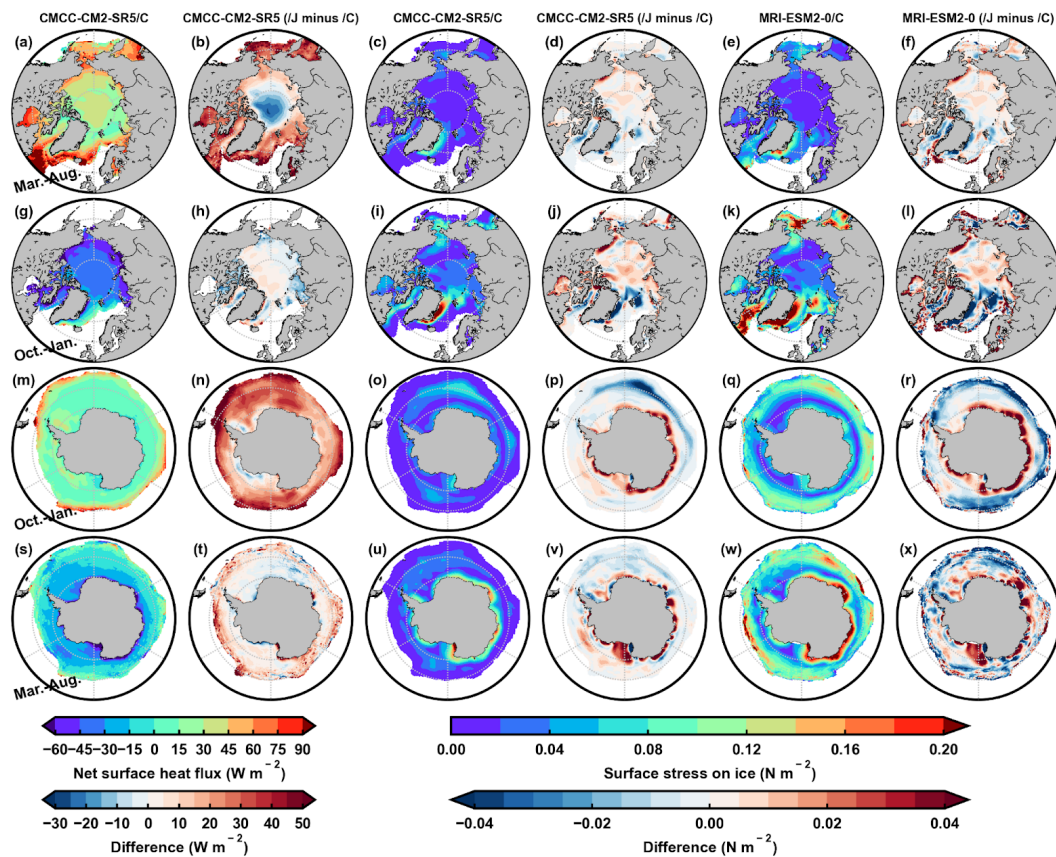
Figure A4. The 1980-2007 March–August and October–January mean Arctic (a to l) and Antarctic (m to x) net surface heat flux (first two columns) and surface stress (last four columns) on sea ice. The first and third columns correspond to CMCC-CM2-SR5/C, and the second and fourth columns are differences between CMCC-CM2-SR5/J and CMCC-CM2-SR5/C. The fifth column corresponds to MRI-ESM2-0/C, and the sixth column is the difference between MRI-ESM2-0/J and MRI-ESM2-0/C. The positive values indicate a net flux downward.
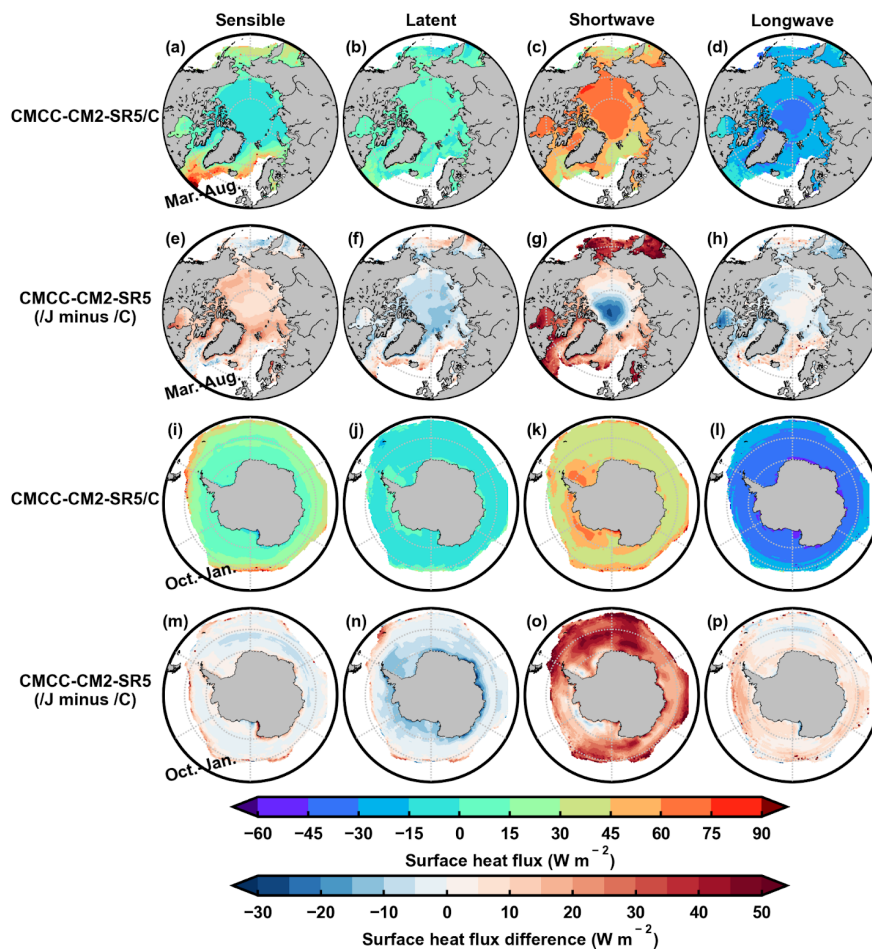
565

Figure A5. The 1980-2007 March-August mean Arctic (a to h) and October-January mean Antarctic (i to p) surface sensible (first column) and latent heat fluxes (second column), net shortwave (third column) and longwave radiation fluxes (fourth column). The first and third rows correspond to CMCC-CM2-SR5/C, and the second and fourth rows are differences between CMCC-CM2-SR5/J and CMCC-CM2-SR5/C. The positive values indicate a net flux
570 **downward.**

28
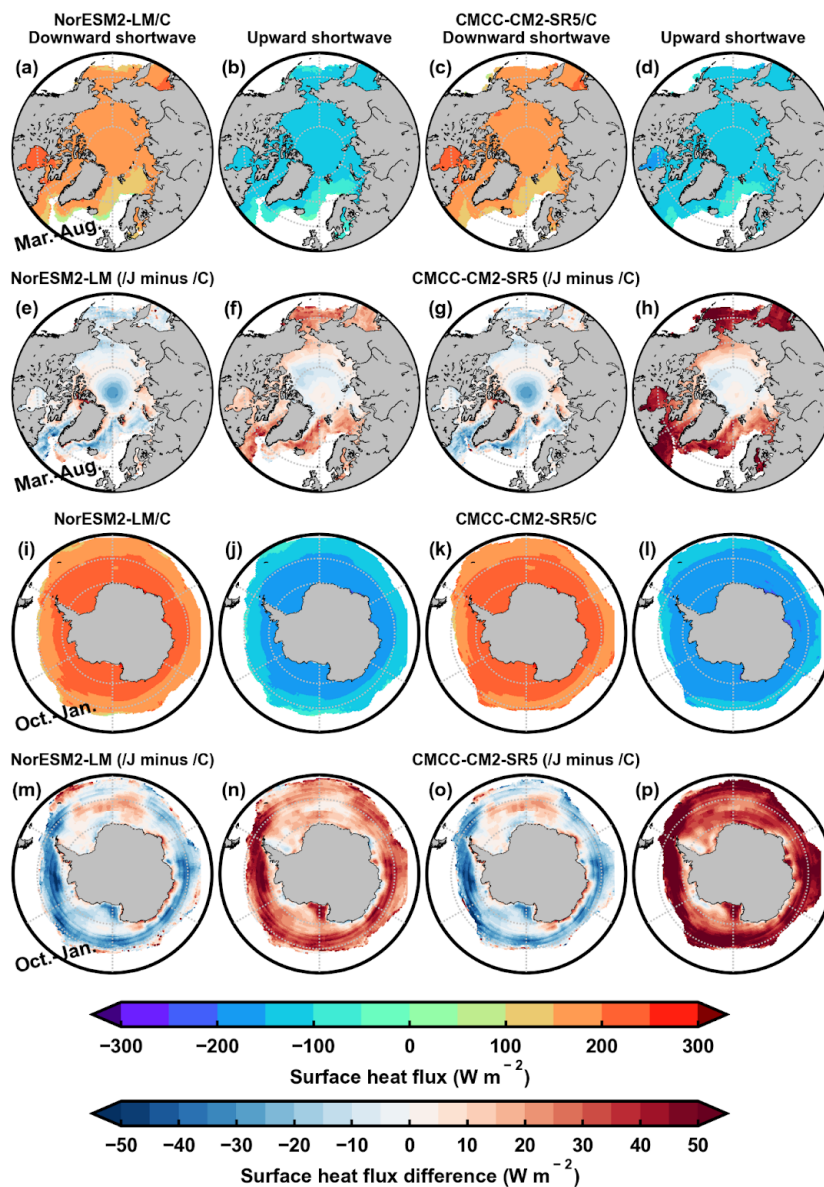
Figure A6. The 1980-2007 March-August mean Arctic (a to h) and October-January mean Antarctic (i to p) downward and upward shortwave radiation fluxes in NorESM2-LM (first two columns) and CMCC-CM2-SR5 (last two columns). The first and third rows correspond to model/C, and the second and fourth rows are differences between model/J and model/C. The positive values indicate a net flux downward.
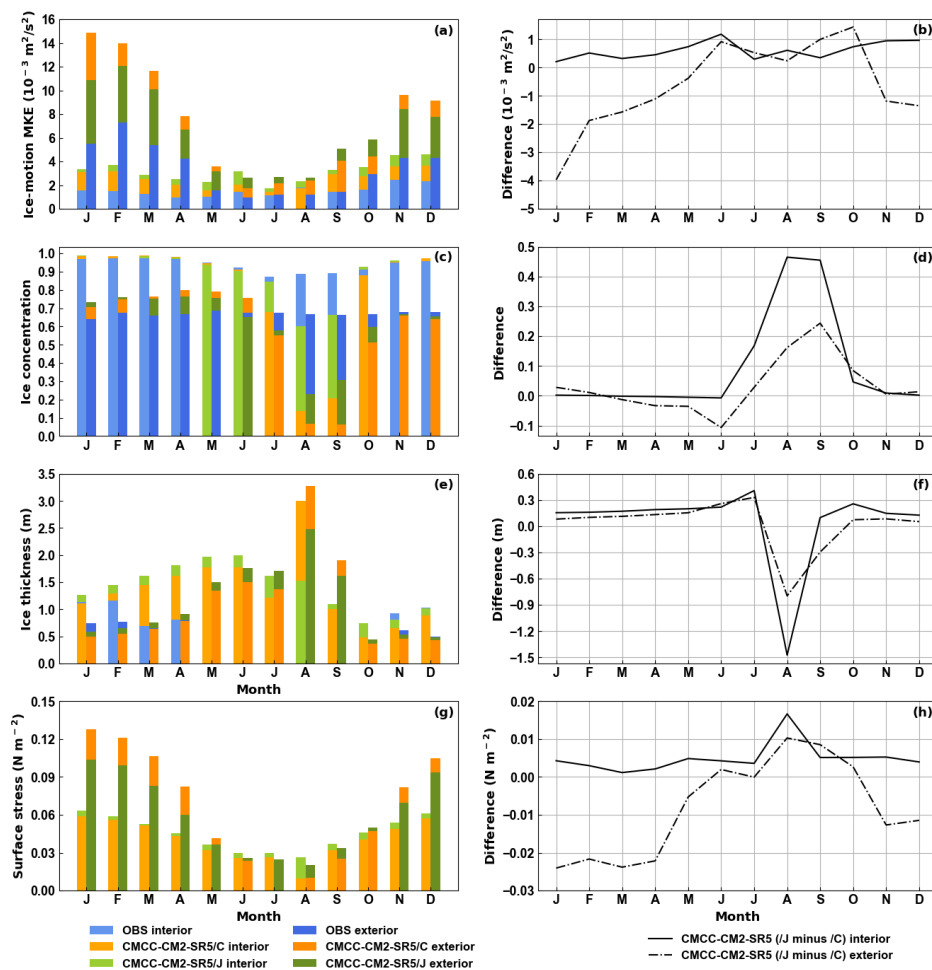
Figure A7. Bar plots of 2003-2007 monthly mean and spatially averaged Arctic ice kinetic energy (MKE) (a), ice concentration (c), ice thickness (e) and surface wind stress (g) from observations (blue), CMCC-CM2-SR5/C (orange), CMCC-CM2-SR5/J (green). These bars all start from zero. The observations of ice MKE, concentration and thickness are derived from KIMURA, NSIDC-0051 and Envisat data, respectively. The Envisat ice thickness data is provided from November to April and the coverage is limited up to 81.5°N. The left (light colors) and right (dark colors) bars of each month are spatial averages on the regions with ice concentration larger (interior) and smaller (exterior) than 80% in NSIDC-0051, respectively. The differences between CMCC-CM2-SR5/J and CMCC-CM2-SR5/C ice MKE (b), ice concentration (d), ice thickness (f) and surface wind stress (h) in the interior (black solid) and exterior (dash-dotted) regions are shown.
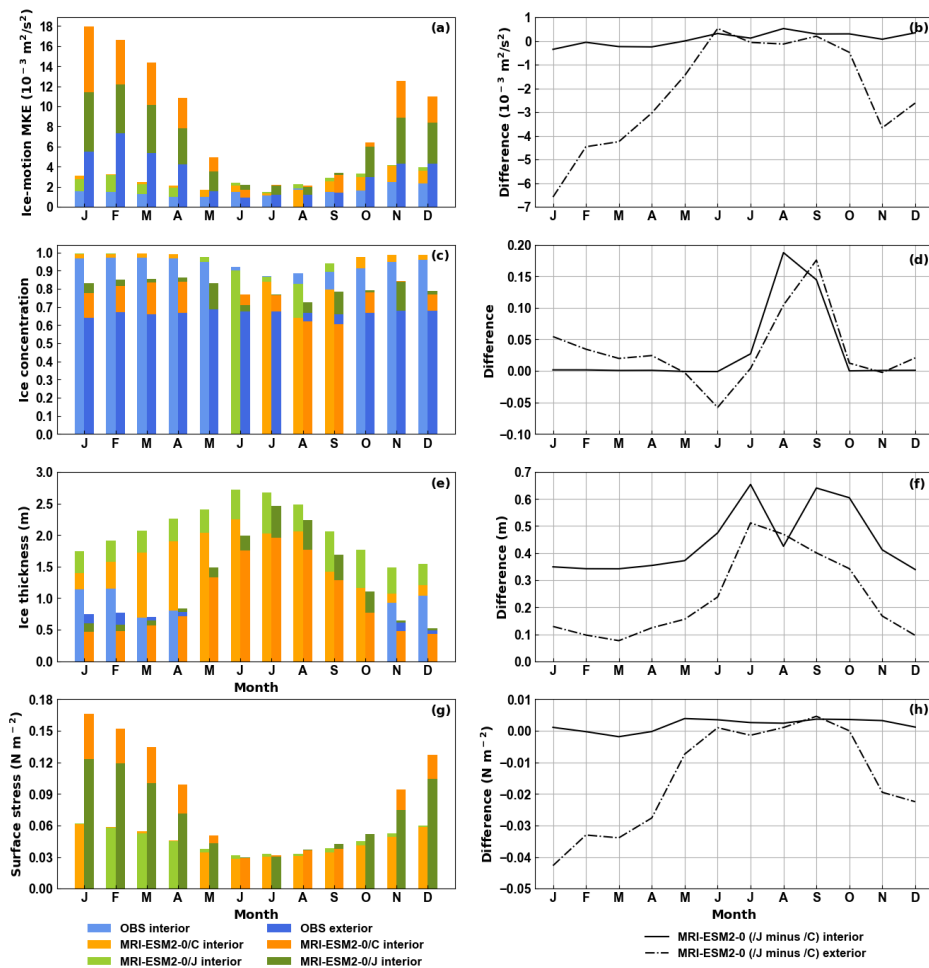
Figure A8. Same as Fig. A7 but for MRI-ESM2-0.
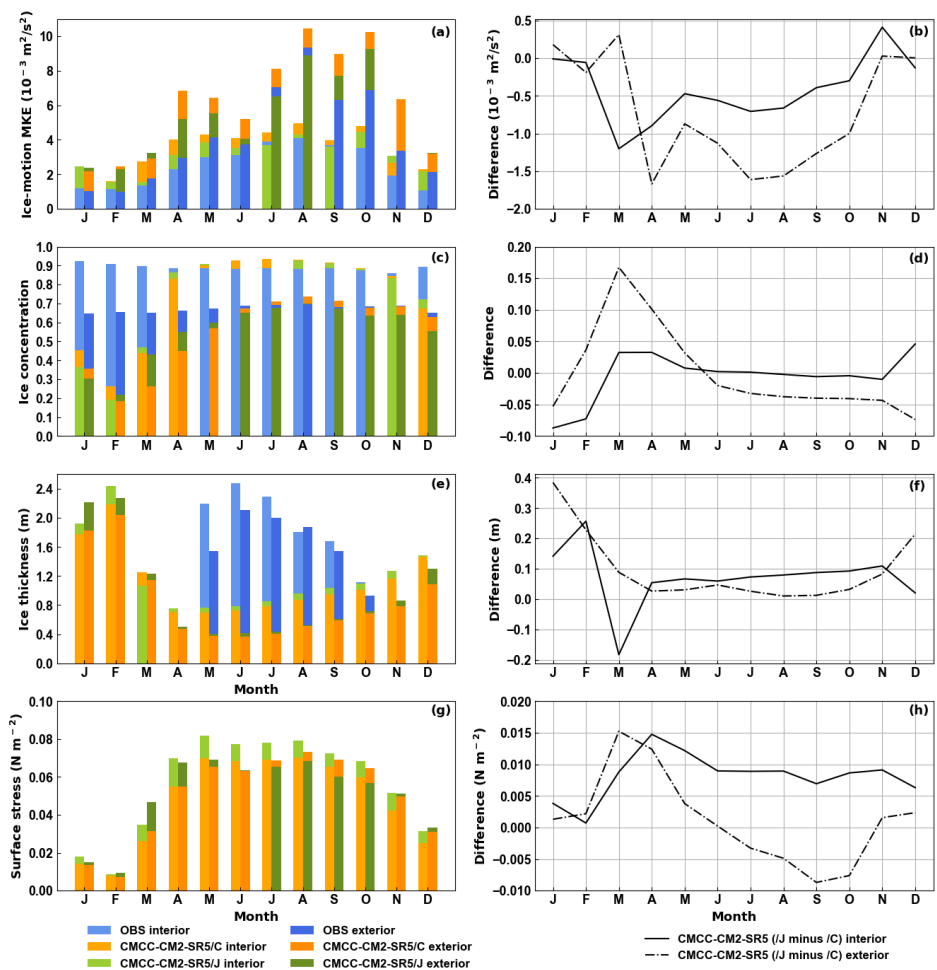
590

Figure A9. Same as Fig. A7 but for CMCC-CM2-SR5 in the Antarctic. The Envisat ice thickness data is provided from May to October.
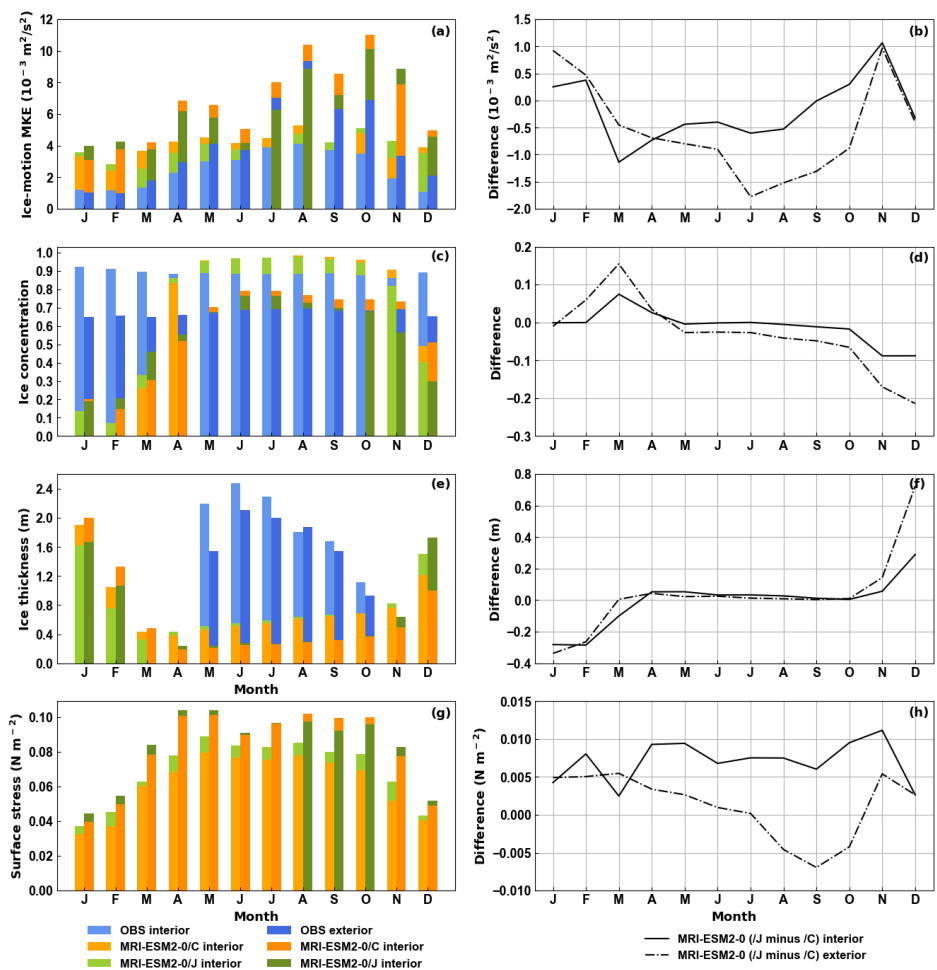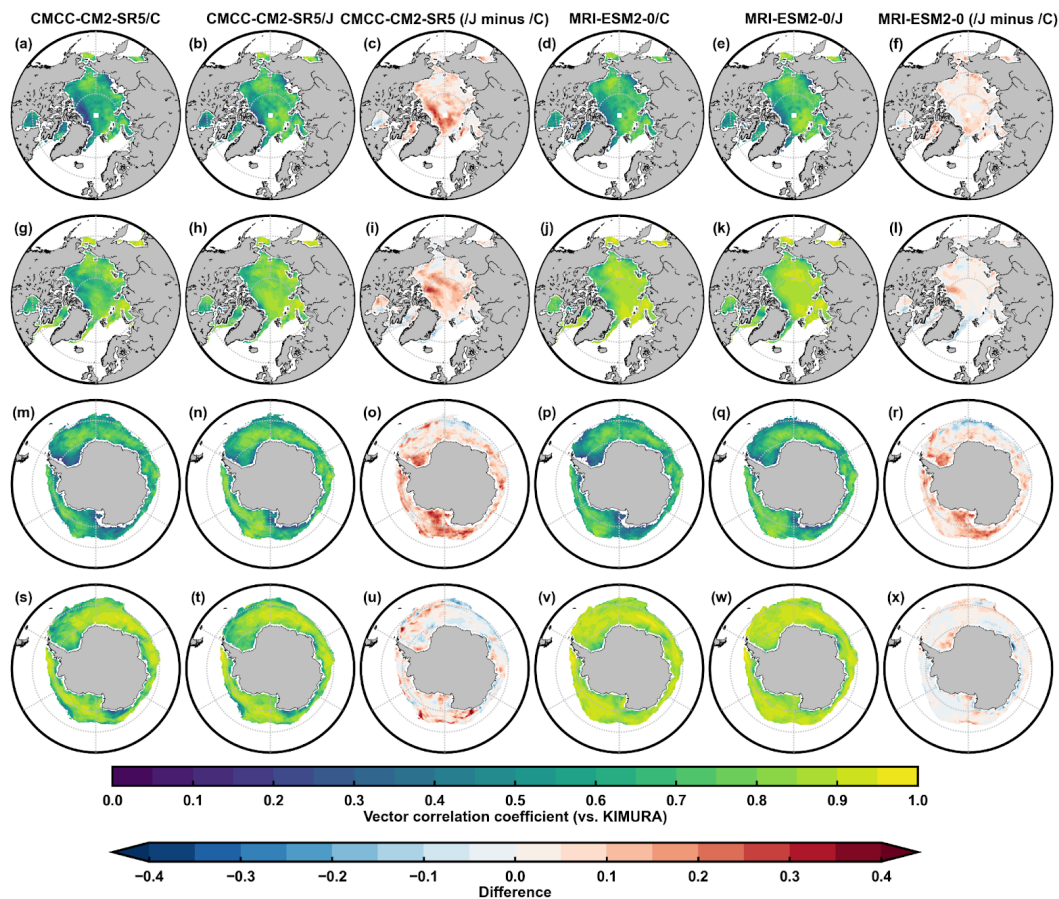
Figure A10. Same as Fig. A9 but for MRI-ESM2-0.

Figure A11. The significant vector correlation coefficients during 2003–2007 at a level of 99% between modeled ice drift (CMCC-CM2-SR5/C or /J, MRI-ESM2-0/C or /J) and KIMURA data in the Arctic (a, b, d, e) and Antarctic (m, n, p, q), and between modeled ice drift and surface wind stress in the Arctic (g, h, j, k) and Antarctic (s, t, v, w). The third and six columns are the differences between the second and first columns, and between the fifth and fourth columns, respectively.

References

Barthélemy, A., Goosse, H., Fichefet, T., and Lecomte, O.: On the sensitivity of Antarctic sea ice model biases to atmospheric forcing uncertainties, Clim. Dyn., 51(4), 1585–1603, doi:10.1007/s00382-017-3972-7, 2018.

Bromwich, D. H., Wilson, A. B., Bai, L. S., Moore, G. W. K., and Bauer, P.: A comparison of the regional Arctic System Reanalysis and the global ERA-Interim Reanalysis for the Arctic, Q. J. R. Meteorol. Soc., 142(695), 644–658, doi:10.1002/qj.2527, 2016.

Cavalieri, D. J., Parkinson, C. L., Gloersen, P., and Zwally, H. J.: Sea Ice Concentrations from Nimbus-7 SMMR and DMSP SSM/I-SSMIS Passive Microwave Data, Version 1, [1980–2007], Boulder, Colorado USA, NASA National Snow and Ice Data Center Distributed Active Archive Center, doi: https://doi.org/10.5067/8GQ8LZQVL0VL, 1996.

Chaudhuri, A. H., Ponte, R. M., and Forget, G.: Impact of uncertainties in atmospheric boundary conditions on ocean model solutions, Ocean Model., 100, 96–108, doi:10.1016/j.ocemod.2016.02.003, 2016.

Chevallier, M., Smith, G. C., Dupont, F., Lemieux, J. F., Forget, G., Fujii, Y., Hernandez, F., Msadek, R., Peterson, K. A., Storto, A., Toyoda, T., Valdivieso, M., Vernieres, G., Zuo, H., Balmaseda, M., Chang, Y. S., Ferry, N., Garric, G., Haines, K., Keeley, S., Kovach, R. M., Kuragano, T., Masina, S., Tang, Y., Tsujino, H., and Wang, X.: Intercomparison of the arctic sea ice cover in global ocean–sea ice reanalyses from the ORA-IP project, Clim. Dyn., 49(3), 1107–1136, doi:10.1007/s00382-016-2985-y, 2017.

Comiso, J. C., Parkinson, C. L., Gersten, R., and Stock, L.: Accelerated decline in the Arctic sea ice cover, Geophys. Res. Lett., 35(1), 1–6, doi:10.1029/2007GL031972, 2008.

Docquier, D., Massonnet, F., Barthélemy, A., Tandon, N. F., Lecomte, O., and Fichefet, T.: Relationships between Arctic sea ice drift and strength modelled by NEMO-LIM3.6, Cryosphere, 11(6), 2829–2846, doi:10.5194/tc-11-2829-2017, 2017.

Eyring, V., Bock, L., Lauer, A., Righi, M., Schlund, M., Andela, B., Arnone, E., Bellprat, O., Carvalhais, N., Cionni, I., Cortesi, N., Crezee, B., L. Davin, E., Davini, P., Debeire, K., De Mora, L., Deser, C., Docquier, D., Earnshaw, P., Ehbrecht, C., K. Gier, B., Gonzalez-Reviriego, N., Goodman, P., Hagemann, S., Hardiman, S., Hassler, B., Hunter, A., Kadow, C., Kindermann, S., Koirala, S., Koldunov, N., Lejeune, Q., Lembo, V., Lovato, T., Lucarini, V., Müller, B., Pandde, A., Phillips, A., Predoi, V., Russell, J., Sellar, A., Serva, F., Stacke, T., Swaminathan, R., Vegas-Regidor, J., Von Hardenberg, J., Weigel, K., and Zimmermann, K.: Earth System Model Evaluation Tool (ESMValTool) v2.0 - An extended set of large-scale diagnostics for quasi-operational and comprehensive evaluation of Earth system models in CMIP, Geosci. Model Dev., 13(7), 3383–3438, doi:10.5194/gmd-13-3383-2020, 2020.

Fogt, R. L., Sleinkofer, A. M., Raphael, M. N., and Handcock, M. S.: A regime shift in seasonal total Antarctic sea ice extent in the twentieth century, Nat. Clim. Chang., 12, 54–62, doi:10.1038/s41558-021-01254-9, 2022.

Griffies, S. M., Danabasoglu, G., Durack, P. J., Adcroft, A. J., Balaji, V., Böning, C. W., Chassignet, E. P., Curchitser, E., Deshayes, J., Drange, H., Fox-Kemper, B., Gleckler, P. J., Gregory, J. M., Haak, H., Hallberg, R. W., Heimbach, P., Hewitt, H. T., Holland, D. M., Ilyina, T., Jungclaus, J. H., Komuro, Y., Krasting, J. P., Large, W. G., Marsland, S. J., Masina, S., McDougall, T. J., George Nurser, A. J., Orr, J. C., Pirani, A., Qiao, F., Stouffer, R. J., Taylor, K. E., Treguier, A. M., Tsujino, H., Uotila, P., Valdivieso, M., Wang, Q., Winton, M., and Yeager, S. G.: OMIP contribution to CMIP6: Experimental and diagnostic protocol for the physical component of the Ocean Model Intercomparison Project, Geosci. Model Dev., 9(9), 3231–3296, doi:10.5194/gmd-9-3231-2016, 2016.

Guerreiro, K., Fleury, S., Zakharova, E., Kouraev, A., Rémy, F., and Maisongrande, P.: Comparison of CryoSat-2 and ENVISAT radar freeboard over Arctic sea ice: Toward an improved Envisat freeboard retrieval, Cryosphere, 11(5), 2059–2073, doi:10.5194/tc-11-2059-2017, 2017.

Haumann, F. A., Gruber, N., Münnich, M., Frenger, I., and Kern, S.: Sea-ice transport driving Southern Ocean salinity and its recent trends, Nature, 537(7618), 89–92, doi:10.1038/nature19101, 2016.

Holland, P. R., and Kwok, R.: Wind-driven trends in Antarctic sea-ice drift, Nat. Geosci., 5(12), 872–
695 875, doi:10.1038/ngeo1627, 2012.

Hu, A., Rooth, C., Bleck, R. and Deser, C.: NAO influence on sea ice extent in the Eurasian coastal
region, Geophys. Res. Lett., 29(22), 10-1-10–4, doi:10.1029/2001gl014293, 2002.

700 Hunke, E. C., and Holland, M. M.: Global atmospheric forcing data for Arctic ice-ocean modeling, J.
Geophys. Res. Ocean., 112(4), doi:10.1029/2006JC003640, 2007.

Kimura, N.: Sea ice motion in response to surface wind and ocean current in the Southern Ocean, J.
Meteorol. Soc. Japan, 82(4), 1223–1231, doi:10.2151/jmsj.2004.1223, 2004.
705

Kimura, N., Nishimura, A., Tanaka, Y., and Yamaguchi, H.: Influence of winter sea-ice motion on
summer ice cover in the Arctic, Polar Res., 32(1), doi:10.3402/polar.v32i0.20193, 2013.

Krikken, F., and Hazeleger, W.: Arctic energy budget in relation to sea ice variability on monthly-to-
710 annual time scales, J. Clim., 28(16), 6335–6350, doi:10.1175/JCLI-D-15-0002.1, 2015.

Large, W. G., and Yeager, S. G.: The global climatology of an interannually varying air-sea flux data
set, Clim. Dyn., 33(2–3), 341–364, doi:10.1007/s00382-008-0441-3, 2009.

715 Lecomte, O., Goosse, H., Fichefet, T., Holland, P. R., Uotila, P., Zunz, V., and Kimura, N.: Impact of
surface wind biases on the Antarctic sea ice concentration budget in climate models, Ocean Model.,
105, 60–70, doi:10.1016/j.ocemod.2016.08.001, 2016.

Lindsay, R., Wensnahan, M., Schweiger, A., and Zhang, J.: Evaluation of seven different atmospheric
720 reanalysis products in the Arctic, J. Clim., 27(7), doi:10.1175/JCLI-D-13-00014.1, 2014.

Lin, X., Zhai, X., Wang, Z., and Munday, D. R.: Mean, variability, and trend of Southern Ocean wind
stress: Role of wind fluctuations, J. Clim., 31(9), 3557–3573, doi:10.1175/JCLI-D-17-0481.1, 2018.

725 Lin, X., Massonnet, F., Fichefet, T., and Vancoppenolle, M.: SITool (v1.0) - a new evaluation tool for
large-scale sea ice simulations: application to CMIP6 OMIP, Geosci. Model Dev., 14(10), 6331–6354,
doi:10.5194/gmd-14-6331-2021, 2021.

Mahlstein, I., Gent, P. R., and Solomon, S.: Historical Antarctic mean sea ice area, sea ice trends, and
730 winds in CMIP5 simulations, J. Geophys. Res. Atmos., 118(11), 5105–5110, doi:10.1002/jgrd.50443,
2013.

Massonnet, F., Fichefet, T., Goosse, H., Vancoppenolle, M., Mathiot, P., and König Beatty, C.: On the
influence of model physics on simulations of Arctic and Antarctic sea ice, Cryosphere, 5(3), 687–699,
735 doi:10.5194/tc-5-687-2011, 2011.

Massonnet, F., Fichefet, T., Goosse, H., Bitz, C. M., Philippon-Berthier, G., Holland, M. M., and
Barriat, P. Y.: Constraining projections of summer Arctic sea ice, Cryosphere, 6(6), 1383–1394,
doi:10.5194/tc-6-1383-2012, 2012.
740

The Cryosphere
Discussions

EGU

Meneghello, G., Marshall, J., Campin, J. M., Doddridge, E., and Timmermans, M. L.: The Ice-Ocean Governor: Ice-Ocean Stress Feedback Limits Beaufort Gyre Spin-Up, Geophys. Res. Lett., 45(20), 11,293-11,299, doi:10.1029/2018GL080171, 2018.

745 Notz, D., and Community, S.: Arctic Sea Ice in CMIP6, Geophys. Res. Lett., 47(10), 1–11, doi:10.1029/2019GL086749, 2020.

Notz, D., Jahn, A., Holland, M., Hunke, E., Massonnet, F., Stroeve, J., Tremblay, B., and Vancoppenolle, M.: The CMIP6 Sea-Ice Model Intercomparison Project (SIMIP): understanding sea ice 750 through climate-model simulations, Geophys. Res. Lett., 9, 3427-3446, doi:10.5194/gmd-9-3427-2016, 2016.

Olason, E., and Notz, D.: Drivers of variability in Arctic sea-ice drift speed, J. Geophys. Res. Ocean., 119(9), 5755–5775, doi:10.1002/2014JC009897, 2014.

755

Parkinson, C. L.: A 40-y record reveals gradual Antarctic sea ice increases followed by decreases at rates far exceeding the rates seen in the Arctic, Proc. Natl. Acad. Sci. U. S. A., 116(29), 14414–14423, doi:10.1073/pnas.1906556116, 2019.

760 Rampal, P., Weiss, J., Dubois, C., and Campin, J. M.: IPCC climate models do not capture Arctic sea ice drift acceleration: Consequences in terms of projected sea ice thinning and decline, J. Geophys. Res. Ocean., 116(9), doi:10.1029/2011JC007110, 2011.

Raphael, M. N., and Hobbs, W.: The influence of the large-scale atmospheric circulation on Antarctic 765 sea ice during ice advance and retreat seasons, Geophys. Res. Lett., 41, 5037–5045, doi:10.1002/2014GL060365, 2014.

Raphael, M. N., and Handcock, M. S.: A new record minimum for Antarctic sea ice, Nat Rev Earth Environ, 3, 215–216, doi:10.1038/s43017-022-00281-0, 2022.
770

Renwick, J. A., Kohout, A., and Dean, S.: Atmospheric forcing of Antarctic sea ice on intraseasonal time scales, J. Clim., 25(17), 5962–5975, doi:10.1175/JCLI-D-11-00423.1, 2012.

Rigor, I. G., Wallace, J. M., and Colony, R. L.: Response of sea ice to the Arctic Oscillation, J. Clim., 775 15(18), 2648–2663, doi:10.1175/1520-0442(2002)015<2648:ROSITT>2.0.CO;2, 2002.

Roach, L. A., Dörr, J., Holmes, C. R., Massonnet, F., Blockley, E. W., Notz, D., Rackow, T., Raphael, M. N., O'Farrell, S. P., Bailey, D. A., and Bitz, C. M.: Antarctic Sea Ice Area in CMIP6, Geophys. Res. Lett., 47(9), 1–10, doi:10.1029/2019GL086729, 2020.
780

Rosenblum, E., and Eisenman, I.: Sea ice trends in climate models only accurate in runs with biased global warming, J. Clim., 30(16), 6265–6278, doi:10.1175/JCLI-D-16-0455.1, 2017.

Sévellec, F., Fedorov, A. V., and Liu, W.: Arctic sea-ice decline weakens the Atlantic Meridional 785 Overturning Circulation, Nat. Clim. Chang., 7(8), 604–610, doi:10.1038/NCLIMATE3353, 2017.

Shu, Q., Song, Z., and Qiao, F.: Assessment of sea ice simulations in the CMIP5 models, Cryosphere, 9(1), 399–409, doi:10.5194/tc-9-399-2015, 2015.

790   Shu, Q., Wang, Q., Song, Z., Qiao, F., Zhao, J., Chu, M., and Li, X.: Assessment of sea ice extent in CMIP6 with comparison to observations and CMIP5, Geophys. Res. Lett., 47(9), 1–9, doi:10.1029/2020GL087965, 2020.

Smith, D. M., Dunstone, N. J., Scaife, A. A., Fiedler, E. K., Copsey, D., and Hardiman, S. C.:
795   Atmospheric response to Arctic and Antarctic sea ice: The importance of ocean-atmosphere coupling and the background state, J. Clim., 30(12), 4547–4565, doi:10.1175/JCLI-D-16-0564.1, 2017.

Smith, D. M., Eade, R., Andrews, M. B., Ayres, H., Clark, A., Chripko, S., Deser, C., Dunstone, N. J., García-Serrano, J., Gastineau, G., Graff, L. S., Hardiman, S. C., He, B., Hermanson, L., Jung, T.,
800   Knight, J., Levine, X., Magnusdottir, G., Manzini, E., Matei, D., Mori, M., Msadek, R., Ortega, P., Peings, Y., Scaife, A. A., Screen, J. A., Seabrook, M., Semmler, T., Sigmond, M., Streffing, J., Sun, L., and Walsh, A.: Robust but weak winter atmospheric circulation response to future Arctic sea ice loss, Nat. Commun., 13(1), 1–15, doi:10.1038/s41467-022-28283-y, 2022.

805   Sterlin, J., Fichefet, T., Massonnet, F., Lecomte, O., and Vancoppenolle, M.: Sensitivity of Arctic sea ice to melt pond processes and atmospheric forcing: A model study, Ocean Model., 167, doi:10.1016/j.ocemod.2021.101872, 2021.

Stroeve, J., and Notz, D.: Changing state of Arctic sea ice across all seasons, Environ. Res. Lett.,
810   13(10), doi:10.1088/1748-9326/aade56, 2018.

Stroeve, J., Barrett, A., Serreze, M., and Schweiger, A.: Using records from submarine, aircraft and satellites to evaluate climate model simulations of Arctic sea ice thickness, Cryosphere, 8(5), 1839–1854, doi:10.5194/tc-8-1839-2014, 2014.
815

Stroeve, J., Holland, M. M., Meier, W., Scambos, T., and Serreze, M.: Arctic sea ice decline: Faster than forecast, Geophys. Res. Lett., 34(9), 1–5, doi:10.1029/2007GL029703, 2007.

Tandon, N. F., Kushner, P. J., Docquier, D., Wettstein, J. J., and Li, C.: Reassessing sea ice drift and its
820   relationship to long-term Arctic sea ice loss in coupled climate models, J. Geophys. Res. Ocean., 123(6), 4338–4359, doi:10.1029/2017JC013697, 2018.

Tsujino, H., Urakawa, S., Nakano, H., Small, R. J., Kim, W. M., Yeager, S. G., Danabasoglu, G., Suzuki, T., Bamber, J. L., Bentsen, M., Böning, C. W., Bozec, A., Chassignet, E. P., Curchitser, E.,
825   Boeira Dias, F., Durack, P. J., Griffies, S. M., Harada, Y., Ilicak, M., Josey, S. A., Kobayashi, C., Kobayashi, S., Komuro, Y., Large, W. G., Le Sommer, J., Marsland, S. J., Masina, S., Scheinert, M., Tomita, H., Valdivieso, M., and Yamazaki, D.: JRA-55 based surface dataset for driving ocean-sea-ice models (JRA55-do), Ocean Model., 130, 79–139, doi:10.1016/j.ocemod.2018.07.002, 2018.

830   Tsujino, H., Shogo Urakawa, L., Griffies, S. M., Danabasoglu, G., Adcroft, A. J., Amaral, A. E., Arsouze, T., Bentsen, M., Bernardello, R., Böning, C. W., Bozec, A., Chassignet, E. P., Danilov, S., Dussin, R., Exarchou, E., Giuseppe Fogli, P., Fox-Kemper, B., Guo, C., Ilicak, M., Iovino, D., Kim, W. M., Koldunov, N., Lapin, V., Li, Y., Lin, P., Lindsay, K., Liu, H., Long, M. C., Komuro, Y., Marsland, S. J., Masina, S., Nummelin, A., Klaus Rieck, J., Ruprich-Robert, Y., Scheinert, M., Sicardi, V., Sidorenko,
835   D., Suzuki, T., Tatebe, H., Wang, Q., Yeager, S. G., and Yu, Z.: Evaluation of global ocean-sea-ice model simulations based on the experimental protocols of the Ocean Model Intercomparison Project phase 2 (OMIP-2), Geosci. Model Dev., 13(8), 3643–3708, doi:10.5194/gmd-13-3643-2020, 2020.

Turner, J., Bracegirdle, T. J., Phillips, T., Marshall, G. J., and Scott Hosking, J.: An initial assessment of
840   Antarctic sea ice extent in the CMIP5 models, J. Clim., 26(5), 1473–1484, doi:10.1175/JCLI-D-12-
00068.1, 2013.

Uotila, P., Holland, P., Vihma, T., Marsland, S., and Kimura, N.: Is realistic Antarctic sea-ice extent in
climate   models   the   result   of   excessive   ice   drift?,   Ocean   Modell.,   79,   33–42,
845   doi:10.1016/j.ocemod.2014.04.004, 2014.

Watts, M., Maslowski, W., Lee, Y. J., Kinney, J. C., and Osinski, R.: A spatial evaluation of Arctic sea
ice and regional limitations in CMIP6 historical simulations, J. Clim., 34(15), 6399–6420,
doi:10.1175/JCLI-D-20-0491.1, 2021.
850

Wu, Y., Wang, Z., Liu, C., and Lin, X.: Impacts of high-frequency atmospheric forcing on Southern
Ocean circulation and Antarctic sea ice, Adv. Atmos. Sci., 37(5), 515–531, doi:10.1007/s00376-020-
9203-x, 2020.

855   Zunz, V., Goosse, H., and Massonnet, F.: How does internal variability influence the ability of CMIP5
models to reproduce the recent trend in Southern Ocean sea ice extent?, Cryosphere, 7(2), 451–468,
doi:10.5194/tc-7-451-2013, 2013.